FABRICATION OF CARBOXYMETHYL CELLULOSE/GELATIN/CALCIUM PHOSPHATE CEMENT/CARBON NANOMATERIAL SCAFFOLDS FOR BONE REGENERATION

by

İlayda Duru

B.S., in Chemistry, Yıldız Technical University, 2013

M.S., in Biomedical Engineering, Boğaziçi University, 2017

Submitted to the Institute of Biomedical Engineering

in partial fulfillment of the requirements

for the degree of

Doctor

of

Philosophy

Boğaziçi University

2023

ACKNOWLEDGMENTS

First of all, I would like to express my sincere gratitude to my advisor Assoc. Prof. Dr. Duygu Ege for her guidance, support and patience. Your guidance and expertise carried me through all the stages of my PhD thesis. I also would like to thank you for your faith in me and including me in your projects and collaborations through these years.

Secondly, I would like to express my sincere gratitude to Assist. Prof. Dr. John Robert Martin for accepting me in his laboratory in Biomedical Engineering in University of Cincinnati. I consider myself so lucky for meeting you and taking your guidance. Thank you for your major contribution to my thesis and also including me to your work and teaching me new scientific methods. I am also so grateful for your meetings and small talks full of motivation. I also want to thank to his PhD students (and my friends) Reinaldo Dos Santos, Dylan Marques and Karina Bruce for their contribution to my PhD thesis, friendship and good time in Cincinnati!

I am also so honored to be able to work in the laboratory of Gamze Torun Köse and taking her guidance. Thank you very much for your contribution to my thesis. I also want to thank to her graduate assistant (and my beautiful friend) Nisa İrem Büyük for her support and contribution to my thesis.

I would like to acknowledge the Scientific and Technological Research Council of Turkey (TUBITAK) for supporting me under 2211A and 2214A programs.

I would like to thank to my thesis progress committee members, Prof. Dr. Bora Garipcan and Prof. Dr. Emin Sünbüloğlu for their contributions and insightful comments on my studies.

It is my pleasure to thank to Prof. Dr. Oktay Demircan for his permission to

use the ball mill in his laboratory and I want to thank to his graduate assistant Ayşenur Eslem Kısa for her support. I also would like to thank to Prof. Dr. Nuri Ersoy for his permission to use the compression test machine in his laboratory and I would like to thank to his graduate assistant Mehmetcan Engül for his support.

I want to thank to my family to encourage me to the academy. Thank you for your endless support! You mean a lot to me!

I would like to thank to my colleagues and friends for their valuable collaboration, support and motivation. Thank you for always being there for me!

Finally, I want to dedicate this thesis to Eren Türkmen. Thank you for walking on this path with me and experiencing academy even it is a completely different field to you. Thank you for being my first listener of my every good or bad experience. Thank you for buying me coffee and walk with me when the things did not go well. Thank you for your endless support and faith in me!

ACADEMIC ETHICS AND INTEGRITY STATEMENT

I, İlayda Duru, hereby certify that I am aware of the Academic Ethics and Integrity Policy issued by the Council of Higher Education (YÖK) and I fully acknowledge all the consequences due to its violation by plagiarism or any other way.

Name :

Signature:

Date:

ABSTRACT

FABRICATION OF CARBOXYMETHYL CELLULOSE/GELATIN/CALCIUM PHOSPHATE CEMENT/CARBON NANOMATERIAL SCAFFOLDS FOR BONE REGENERATION

Compressive strength and inherent osteogenic capacity of calcium phosphate cements (CPCs) remain relatively limited. In this thesis, first, powder and liquid phase of CPCs were optimized. After this, nanodiamond (ND) and Fullerenol (Ful) were incorporated into carboxymethyl cellulose/gelatin (CMC/Gel) CPCs to enhance their ability to promote compressive strength and bone formation, respectively. It was found that ND did not contribute to the compressive strength of CPCs in unfunctionalized form; however, it was efficient to reduce the setting time of cements. Besides ND, the biocompatible Ful particles were introduced into CPCs at concentrations of 0.02, 0.04, and 0.1 wt/v%. The addition of Ful at the highest concentration to CMC/Gel cements leaded to a decrease in setting times, attributed to enhanced hydrogen bonding facilitated by the hydroxyl groups of Ful. *In vitro* studies focusing on reactive oxygen species (ROS) scavenging demonstrated the antioxidant activity when Ful was incorporated into CMC/Gel cements and the scavenging capacity of the cement was highest for 0.02 and 0.04 wt/v% Ful concentrations. Additionally, *in vitro* cytotoxicity studies revealed that cements with 0.02 and 0.04 wt/v% Ful protected cellular viability. Furthermore, treating MC3T3-E1 pre-osteoblast cells with low-dose Ful cements leaded to an increase in osteogenic differentiation. These findings strongly suggest a correlation between the osteogenic abilities of Ful-loaded cements and their antioxidant activity levels. Thus, this study highlights the promising potential of ND and Ful for enhancing the performance of CPCs in bone reconstruction procedures.

Keywords: Calcium Phosphate Cement, Fullerenol, Antioxidant, Nanodiamond, Bone.

ÖZET

KEMİK YENİLENMESİ İÇİN KARBOKSİMETİL SELÜLOZ/JELATİN/KALSİYUM FOSFAT ÇİMENTO/KARBON NANOMALZEME DOKU İSKELELERİNİN ÜRETİMİ

Kalsiyum fosfat çimentoların (CPCler) basma dayanımı ve osteojenik özellikleri yetersizdir.Bu tezde ilk olarak, CPClerin toz ve sıvı fazları optimize edilmiştir. Daha sonra, nanoelmas (ND) ve Fullerenol (Ful) karboksimetil selüloz/jelatin çimentolara sırasıyla basma dayanımı ve kemik oluşumunu arttırmak amacıyla eklenmiştir. Sonuçlara göre ND, CPClerin basma dayanımına etki etmemiş olup çimentoların katılaşma süresini azaltmıştır. ND'den farklı olarak Ful, çimentolara ağırlık/hacimce % 0.02, 0.04 ve 0.1 oranlarında eklenmiştir. Yüksek oranda Ful eklenmesi, çimentonun katılaşma süresini düşürmüştür ve bu da Ful'un hidroksil gruplarının hidrojen bağı yapmasıyla açıklanabilir. Reaktif oksijen türlerini tutabilme üzerine yapılan *in vitro* calışmalar, Ful'un çimentolara antioksidan özellik kattığını göstermiş ve en yüksek antioksidan özellikler ağırlık/hacimce % 0.02 ve 0.04 Ful konsantrasyonlarında görülmüştür. Ayrıca *in vitro* sitotoksisite çalışmaları, bu konsantrasyonların hucre canlılığını koruduğunu göstermiştir. Hatta bu konsantrasyonlarda Ful eklenmesi ile MC3T3-E1 pre-osteoblast hücrelerinin, osteojenik farklılaşması artmıştır. Bu sonuçlar, Ful katkılı çimentoların antioksidan aktivitesi ile osteojenik yeterlilikleri arasında bir ilgi olduğunu gostermiştir. Özetle bu calışma, CPC'lerin kemik oluşum uygulamalarindaki performansına ND ve Ful'un önemli etkisini ortaya koymaktadır.

Anahtar Sözcükler: Kalsiyum Fosfat Çimento, Fullerenol, Antioksidan, Nanoelmas, Kemik

TABLE OF CONTENTS

LIST OF FIGURES

LIST OF TABLES

LIST OF SYMBOLS

A_{Ful}	Absorbance of DPPH solutions with Ful containing cements
$A_{CMC/Gel}$	Absorbance of DPPH solutions with CMC/Gel containing cements
$Ca_4(PO_4)_2O$	Tetracalcium phosphate
$CaHPO_4$	Dicalcium phosphate anhydrous
$CaHPO_4.2H_2O$	Dicalcium phosphate dihydrate
α-$Ca_3(PO_4)_2$	α-Tricalcium phosphate
$Ca(H_2PO_4)_2 \cdot H_2O$	monocalcium phosphate monohydrate
$Ca_{10}(PO_4)_6(OH)_2$	Hydroxyapatite
$Ca_9(HPO_4)(PO_4)_5OH$	Calcium-deficient hydroxyapatite
Ca^{+2}	Calcium ion
Sr^{+2}	Strontium ion
Mg^{+2}	Magnesium ion
$C_{60}(OH)_n$	Fullerenol
Na_2HPO_4	Disodium hydrogen phosphate
$CaSO_4$	Calcium sulphate
g	gram
MPa	Mega Pascals
GPa	Giga Pascals
nm	nanometer
μm	micrometer
μL	microliter
wt/v%	weight/volume%
M	Molar
$^{\circ}C$	Degree Celcius

LIST OF ABBREVIATIONS

ALP	Alkaline phosphatase
BMP-2	Bone morphogenetic protein-2
CDHA	Calcium-deficient hydroxyapatite
CMC	Carboxymethyl cellulose
CPC	Calcium phosphate cement
DPPH	1,1-Diphenyl-2-picrylhydrazine
ECM	Extracellular matrix
EDX	Energy dispersive X-ray spectroscopy
FITC	Fluorescein 5-isothiocyanate
FTIR	Fourier Transform Infrared Spectroscopy
Ful	Fullerenol
Gel	Gelatin
HA	Hydroxyapatite
MSC	Mesenchymal stem cell
ND	Nanodiamond
PBS	Phosphate buffered saline
PDGF	Platelet-derived growth factor
PLLA	Poly(L-Lactic acid)
PMMA	Polymethylmethacrylate
PVDF	Polyvinylidene fluoride
ROS	Reactive oxygen species
Runx2	Runt-related transcription factor 2
SBF	Simulated body fluid
SEM	Scanning electron microscopy
XRD	X-ray diffraction

1. INTRODUCTION

1.1 Motivation

Unlike highly exothermic polymethylmethacrylate (PMMA) cements that can generate heat and harm nearby tissues, CPCs can produce apatite under physiological conditions without causing any damage [1, 2]. However, the clinicians suffer from their obstructions. Lack of cohesiveness and disintegration of cements limit the applicability of CPCs [3, 4, 5]. Moreover, CPCs are brittle and low compressive strength restricts their utility to non-load bearing areas [3, 6]. Finally, osteogenic ability of CPCs are inadequate and low osteogenic ability limits the applications of CPCs, especially in osteoporotic bones [3, 7, 8].

The prominent materials which CPCs are combined with are naturally-derived polymers like carboxymethyl cellulose (CMC) and gelatin (Gel). CMC is known to improve overall handling by increasing material viscosity [3, 9], and enhancing the wash-out resistance [3, 4] while Gel is reported as an efficient agent to boost the compressive strength and modulus of CPCs [6, 10]. Moreover, several materials have been proposed as potential additives to enhance the osteogenic ability of CPCs. The most extensively studied additives for this purpose are therapeutic growth factor proteins. However, these recombinant proteins are expensive and difficult to use in a heterogenous patient population that often requires varying dosages [11, 12]. Furthermore, the use of BMP-2 in the clinic has been associated with disadvantages including ectopic bone formation and excessive inflammation [12, 13]. Despite the handling issue of CPCs seems to be solved with wash-out agents, the compressive strength and osteogenic ability of CPCs still need to be improved. The fundamental motivation of this thesis is improving compressive strength and osteogenic ability of CMC/Gel-incorporated CPCs.

1.2 Objectives and Outline of the Thesis

For enhancing compressive strength of CPCs, nanodiamond (ND) is investigated. Moreover, a biocompatible antioxidant, Fullerenol (Ful), is incorporated to cements for accelerating and increasing the osteogenic differentiation, which is an underexplored strategy. Besides the targeted properties of cements, the physical characteristics of CPCs including setting time, apatite formation and apatite morphology were all studied. The main goal of my PhD thesis is to heighten the compressive strength and osteogenic ability of CPCs while improving (or without compromising) the physical cement properties.

- Presenting the motivation and literature review related to this thesis

The motivation and objectives of this thesis work was presented in the Chapter 1. Background information on bone tissue engineering, CPCs and additives were explained in Chapter 2.

- Developing ND and Ful-incorporated CPCs

For this purpose, the particle size of powder phase and pH of liquid phase were optimized. The optimization studies were explained in Chapter 3. In Chapter 4, the effect of ND on compressive strength and physical characteristics of CPCs was presented. In Chapter 5, the effect of Ful on physical characteristics, cell viability and osteogenic ability was demonstrated. Finally, all the findings of this thesis were summarized in Chapter 6.

2. BACKGROUND

2.1 Bone Structure and Remodeling

To develop scaffolds repairing bone defects, it is essential to understand the bone structure. Figure 2.1 illustrates bone structure.

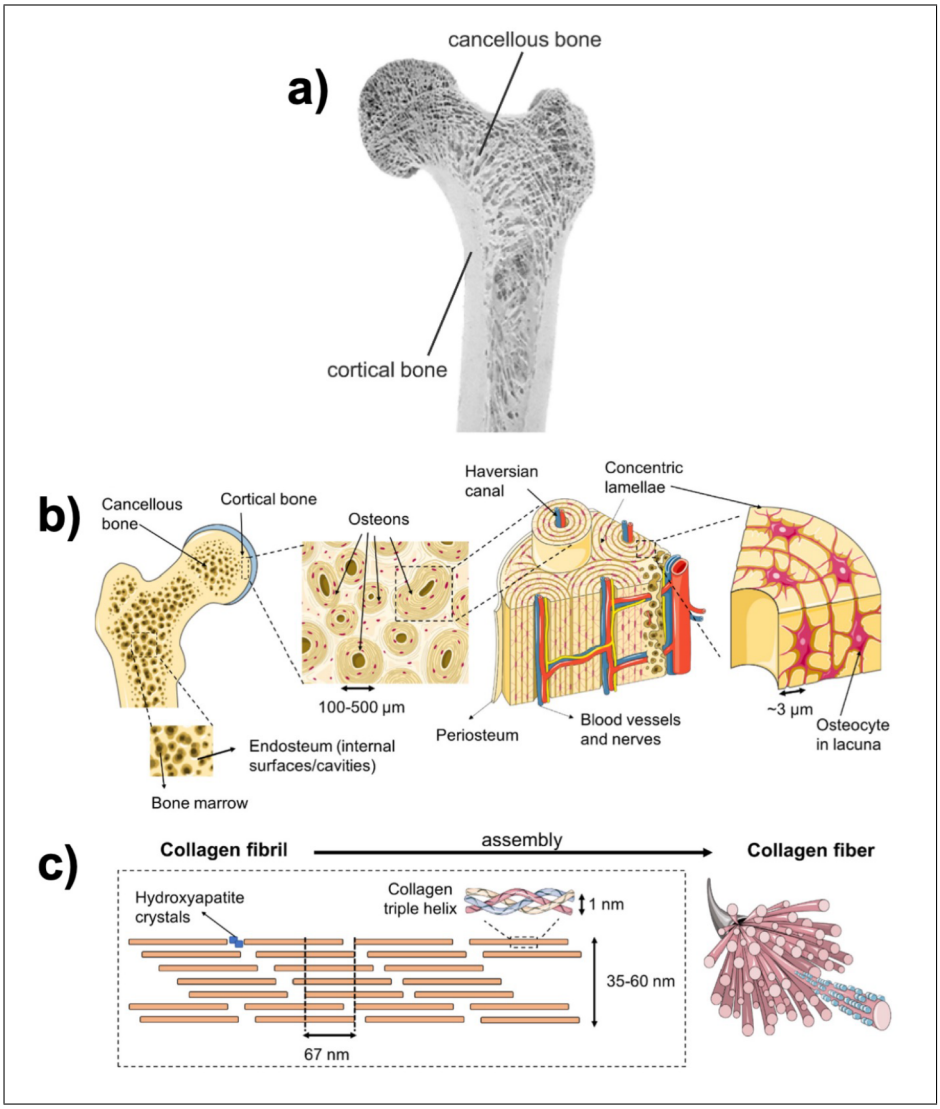

Figure 2.1 (a) The main structure of bone[14] (b) Hierarchical structure of bone (c) Collagen fibrils assembling to collagen fibers and hydroxyapatite (HA) crystals located in the gaps [15].

Cortical bone is sourced from osteons which are also called Haversian systems. Osteons consist of concentric circles of lamellae which are about 3 μm thick and en-

circling a Haversian canal, which accomodates nerves and blood vessels [15, 16]. The inner section is in close proximity to the blood vessel canals, the bone marrow cavity and comprises osteoblasts, osteoclasts and blood vessels. Cancellous bone consists of a lattice-like arrangement of trabecular plates, resembling a honeycomb structure. This configuration renders the bone porous and lightweight, yet resistant to forces. The interstitial spaces among the trabeculae also accommodate bone marrow [15, 16].

In a nanoscopic level, bone is composed of numerous structural proteins and polysaccharides, primarily consisting of collagen fibrils. These fibrils are arranged in a periodicity of 67 nm with gaps of 40 nm and are mineralized by HA crystals that are anisotropic and incredibly rigid. The HA crystals are found within the collagen gaps and makes up 70% of bone [15].

Cortical bone and cancellous bone are mechanically different. Cancellous bone is highly porous and has low density. It exhibits high elasticity, resilience and toughness due to its organic constituents. On the other hand, cortical tissue is denser than cancellous bone and provides protection for the inner cancellous tissue. Due to its lack of organic matter and greater mineralization content, cortical tissue is stiffer, has lower toughness and higher elastic modulus [16]. Table 2.1 summarizes these properties [16, 17, 18].

Table 2.1
Mechanical parameters of cancellous and cortical bone.

	Cancellous Bone	Cortical Bone
Compressive strength (MPa)	2-12	130-225
Compressive modulus (GPa)	0.12-1.1	3-30

The integrity of bone tissue is maintained by bone remodeling and it is depicted in Figure 2.2.

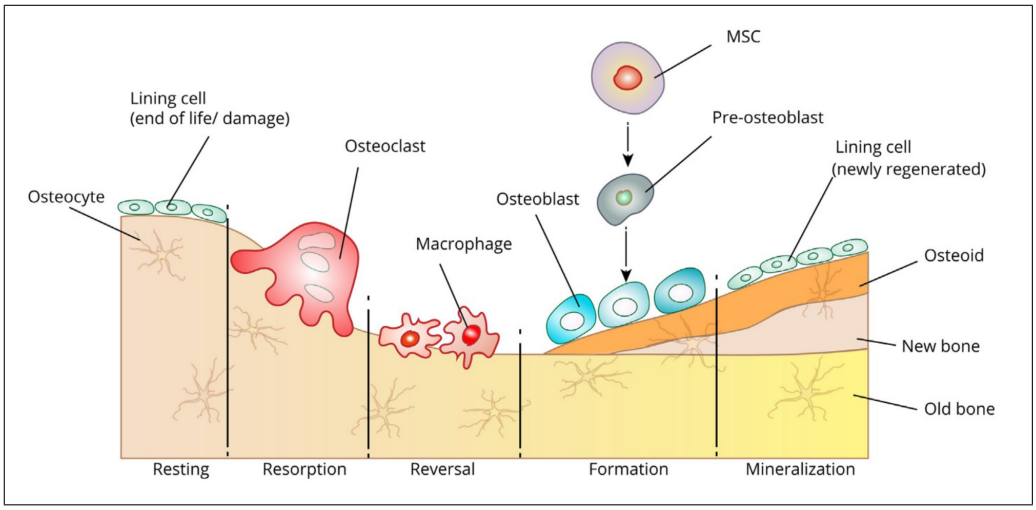

Figure 2.2 Bone remodeling process [16].

Osteoblasts and osteoclasts engage in cross-communication to maintain bone homeostasis. During the process of bone regeneration, osteoclasts break down the old tissue and this exposes essential ions and minerals necessary for bone formation. This is followed by the recruitment of osteoblasts to facilitate bone formation and mineralization[16].

Regeneration in most bones including the long bones of the ribs and limbs starts with endochondral ossification. The differentiation of MSCs into chondrocytes starts the endochondral ossification and a cartilaginous tissue with a separate extracellular matrix (ECM) is formed. The chondrocytes subsequently differentiate into hypertrophic chondrocytes, which undergo resorption and replacement by bone marrow when engulfed by specialized cells (osteoclasts and osteoblast progenitors) and

blood vessels. Afterwards, osteoblast progenitors differentiate into osteoblast cells that synthesize a mixture of ECM proteins, including alkaline phosphatase (ALP), osteocalcin and a significant amount of type I collagen. Subsequently, calcium phosphates accumulate in the form of HA within the collagen-proteoglycan in osteoid, resulting in a composite organic and inorganic phase. Ultimately, the osteoblast cells become enclosed by the layers of the outer calcified shell and the osteoid matrix, resulting in the development of osteocyte cells[16].

2.2 Wound Healing Process

Wound healing process contains various molecular and cellular activities that require appropriate ECM. It consists of four phases: the inflammatory phase, followed by two repair phases that involve the formation of soft and hard calluses, and finally the remodeling phase [16]. At first stage, platelets are the initial providers of mitogenic factors at an injured location. In addition to coagulation factors, they secrete growth factors which encourage the bone regeneration. Moreover, MSCs in the cambium layer of the endosteum, periosteum, bone marrow, and nearby soft tissues start to proliferate at this stage [19]. Stages of soft and hard tissue formation basically involve endochondral ossification and these stages are explained in Section 2.1 with the final stage of wound healing which is bone remodeling.

2.3 Bone Tissue Engineering

The reason of extensive bone loss is trauma or disease and bone loss leads to musculoskeletal disorders. Creating a scaffold that can effectively treat significant load-bearing bone defects is a significant challenge [20]. A critical-sized gap of at least 3 cm is defined as a large bone defect [21]. The current clinical solution is autologous bone grafting, which can induce bone regeneration and provide high strength standard for these defects and bioactivity. However, autografts have disadvantages including

donor site morbidity, insufficient supply and high graft resorption rates. While allografts which are transplanted tissues from other humans can address some of these disadvantages, they often have low integration with native bone, resulting in reduced strength and bioactivity. Hence, synthetic bone substitutes are heavily investigated as alternatives to autografts and allografts [21, 22].

A synthetic bone graft must possess the advantageous characteristics of an autograft, such as exhibiting high mechanical strength and providing sustained support after implantation in a load-bearing defect. Additionally, it must be osteoconductive and preferably osteoinductive to induce bone formation. Finally, a bone graft must be reproducible through a controlled manufacturing process[20].

2.4 Calcium Phosphate Cements

Four decades ago, Brown and Chow invented the moldable calcium phosphates which are called calcium phosphate cements (CPCs) [23, 24]. The introduction of CPCs has led to the development of more than a dozen commercial CPC formulations [25]. Due to their moldability, they are easily applied to osseous defects and they have been extensively used as bone substitutes in clinical applications for more than two decades [26, 27, 28]. Unlike highly exothermic PMMA cements that generate heat and harm nearby tissues, CPCs produce apatite in physiological conditions without causing any harm.

CPCs produce apatite or brushite ($CaHPO_4.2H_2O$, dicalcium phosphate dihydrate, DCPD) from initial calcium phosphates in physiological conditions [29]. Respective equations are given below:

$$2\,Ca_4(PO_4)_2O + 2\,CaHPO_4 \longrightarrow Ca_{10}(PO_4)_6(OH)_2 \quad (1)\ [29]$$

$$2\,Ca_4(PO_4)_2O + 2\,CaHPO_4 \cdot 2\,H_2O \longrightarrow Ca_{10}(PO_4)_6(OH)_2 + 4\,H_2O \quad (2)\ [30]$$

$$1.5\,Ca_4(PO_4)_2O + 3\,CaHPO_4 \longrightarrow Ca_9(HPO_4)(PO_4)_5OH + 0.5\,H_2O \quad (3)\ [31]$$

$$1.5\,Ca_4(PO_4)_2O + 3\,CaHPO_4 \cdot 2\,H_2O \longrightarrow Ca_9(HPO_4)(PO_4)_5OH + 6.5\,H_2O \quad (4)\ [30]$$

$$3\text{-}\alpha Ca_3(PO_4)_2 + H_2O \longrightarrow Ca_9(HPO_4)(PO_4)_5OH \quad (5)\ [29]$$

$$\alpha\text{-}Ca_3(PO_4)_2 + Ca(H_2PO_4)_2 \cdot H_2O + 7\,H_2O \longrightarrow 4\,CaHPO_4 \cdot 2\,H_2O \quad (6)\ [29]$$

The first two reactions relate to the original composition proposed by Brown and Chow, in which basic tetracalcium phosphate ($Ca_4(PO_4)_2O$, TTCP) reacts with neutral dicalcium phosphate anhydrous ($CaHPO_4$, DCPA) or DCPD and water to form slightly basic HA [32]. Calcium-deficient HA (CDHA) can also be synthesized when the molar ratios of TTCP and DCPA or DCPD are altered as demonstrated in Equation 3 and 4, respectively. Most commercial cement formulations employ the fifth reaction, in which slightly basic α-tricalcium phosphate (α-$Ca_3(PO_4)_2$, α-TCP) transforms via dissolution-precipitation into slightly basic calcium-deficient HA, without any alteration in pH [29]. Equation 6 shows the synthesis of brushite via the reaction of acidic monocalcium phosphate monohydrate ($Ca(H_2PO_4)_2 \cdot H_2O$, MCPM) and basic α-TCP and and water [29].

2.4.1 Additives to Calcium Phosphate Cements

Various materials are incorporated to CPCs to enhance their handling properties, compressive strength and osteogenic ability. The poor properties of cements and mainly used materials to address these properties are explained in the sections below which are 2.4.1.1, 2.4.1.2 and 2.4.1.3.

2.4.1.1 Handling Properties of Calcium Phosphate Cements. Handling properties of CPCs mainly point out the integration of the cement [4]. CPC must be

cohesive enough to prevent disintegration in the body. Disintegration of the cement was reported to cause cement embolism, leading to cardiovascular complications [5]. Enhancing the integration of cements is possible via increasing the immobilization of powder phase with viscous agents in liquid phase [3, 4]. Cellulose derivatives such as hydroxypropyl methylcellulose and carboxymethyl cellulose (CMC) are efficient to increase the handling properties of CPCs [3, 4]. Indeed, CMC is a widely used non-toxic pharmaceutical additive [9] and numerous studies showed its efficiency to increase the handling properties of cements without compromising compression strength and bone forming ability [4, 9].

2.4.1.2 Compressive Strength of Calcium Phosphate Cements. Poor compressive strength restricts the applications of CPCs. The addition of a polymer to CPCs improves their ductility, enabling them to undergo greater deformation before fracturing. Furthermore, the reinforcement of cements with polymers has been widely investigated as a means of enhancing their compressive strength [33]. Among these polymers, gelatin (Gel) is the prominent polymer. The studies showing Gel's effect on CPCs' compressive strength is presented in Figure 2.3.

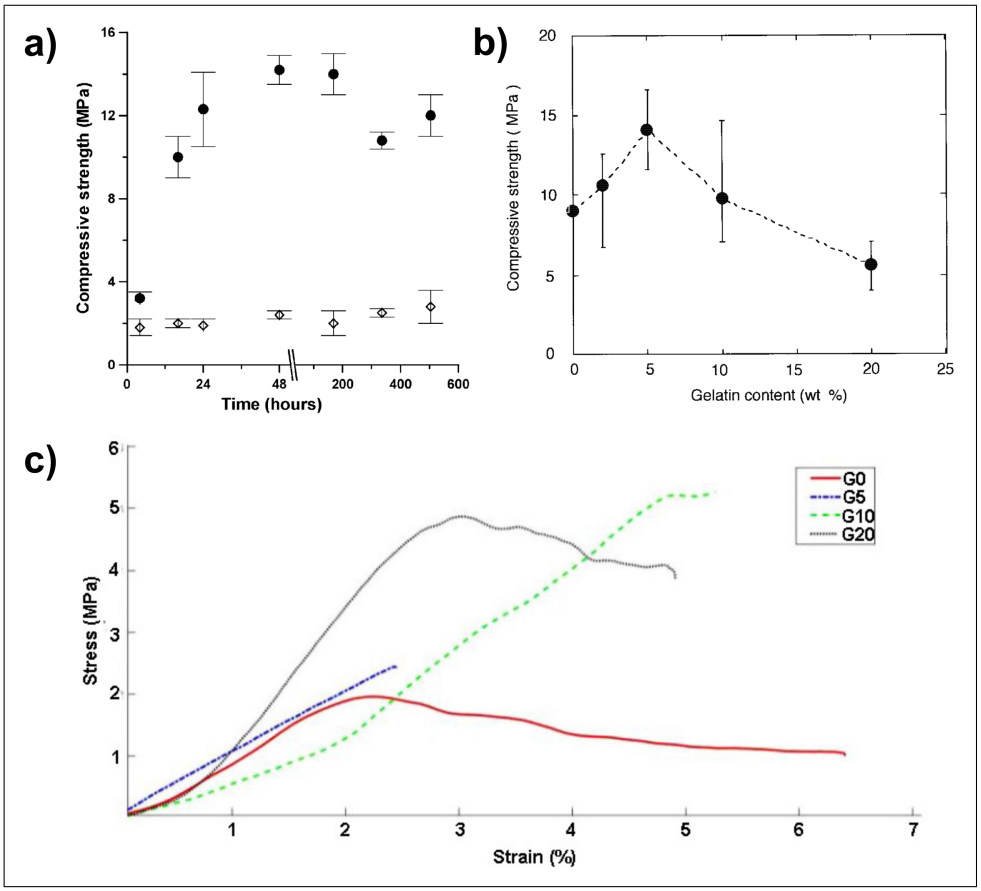

Figure 2.3 a) The effect of Gel on compressive strength of CPCs at different time points (white bullets: CPCs without gelatin, dark bullets: CPCs with gelatin) [34] b) The change of compressive strength of CPCs via addition of different amount of Gel [35] c) Stress-strain graphs of CPCs containing different amount of Gel [10].

As demonstrated in Figure 2.3, Gel improves the compressive strength of CPCs as observed in numerous studies [6, 10]. Indeed, Bigi et al. [6] demonstrated that adding Gel to CPCs can enhance their compressive strength to up to five times greater than unmodified cements. It is also significant to note that high concentrations of Gel such as 10 wt% or 20 wt% deteriorate the compressive strength of cements due to macropore formation with rapid degradation of Gel.

In addition to Gel, chitosan and alginate have been studied to increase compressive strength of CPCs [36, 37, 38]. The reason for the contribution of Gel, chitosan and alginate on compressive strength of CPCs was explained as filling the micropores of cements by polymer [6] or the interaction between the chemical groups and Ca^{+2} ions [37]. Finally, Gel has been reported favorable among these polymers since its RGD

(Arginine-Glycine-Aspartic acid) sequence facilitate cell attachment and proliferation [3, 6].

2.4.1.3 Osteogenic Ability of Calcium Phosphate Cements. Various materials have been suggested as additives to CPCs to enhance the bone forming ability of calcium phosphate cements. Growth factors are used in osteoinductive grafts [7, 39]. Indeed, recombinant BMP-2 is Food and Drug Administration-approved growth factor utilized clinically [40]. However, these recombinant proteins are expensive and challenging to supply from a naturally heterogeneous patient population that often requires variable dosing of these compounds [11, 12]. Additionally, the clinical use of BMP-2 has been attributed to drawbacks such as ectopic bone formation and excessive inflammation [12, 13].

Bioactive ions such as Sr^{+2} [41] and Mg^{+2} [42] have been investigated as pro-osteogenic additives to CPCs. Wu et al. [41] reported that Sr^{+2} enhanced the COL-1 level. Moreover, Ding et al. [42] observed that Mg^{+2} upregulated the BMP-2 activity. Recently, studies have also revealed that CPCs loaded with magnetic nanoparticles (reduced graphene oxide, iron oxide) and exposed to electromagnetic fields can boost the osteogenesis of stem cells [1, 43]. Nevertheless, despite these diverse strategies employed to enhance the osteogenesis on CPCs, their efficacy in clinical bone reconstruction procedures remains unproven.

2.5 Carbon Nanomaterials

2.5.1 Nanodiamond

Nanodiamond (ND) is one of the prominent carbon nanomaterials. The basic component of ND is sp^3 carbon and it also has an outer shell with functional groups sourced from the synthesis process of ND [44]. ND's chemical streucture is presented in Figure 2.4.

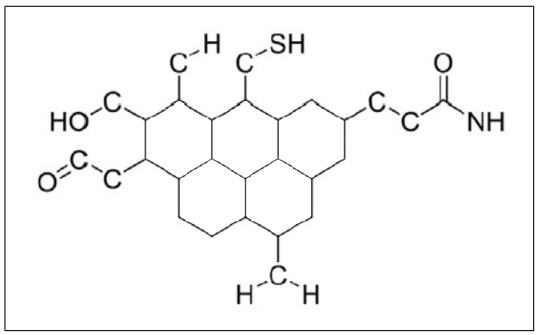

Figure 2.4 ND's chemical structure [44].

Among the various carbon nanomaterials, nanodiamond (ND) has received significant attention in medical research due to its biocompatibility, chemical stability and superior hardness [45, 46]. It has been studied in polymeric scaffolds and blended with both synthetic and natural polymers including poly(lactic-co-glycolic acid), polycaprolactone and gelatin [45, 46, 47, 48, 49, 50, 51, 52, 53, 54, 55, 56, 57, 58]. Figure 2.5 illustrates how the incorporation of ND increases the mechanical strength of polymeric scaffolds.

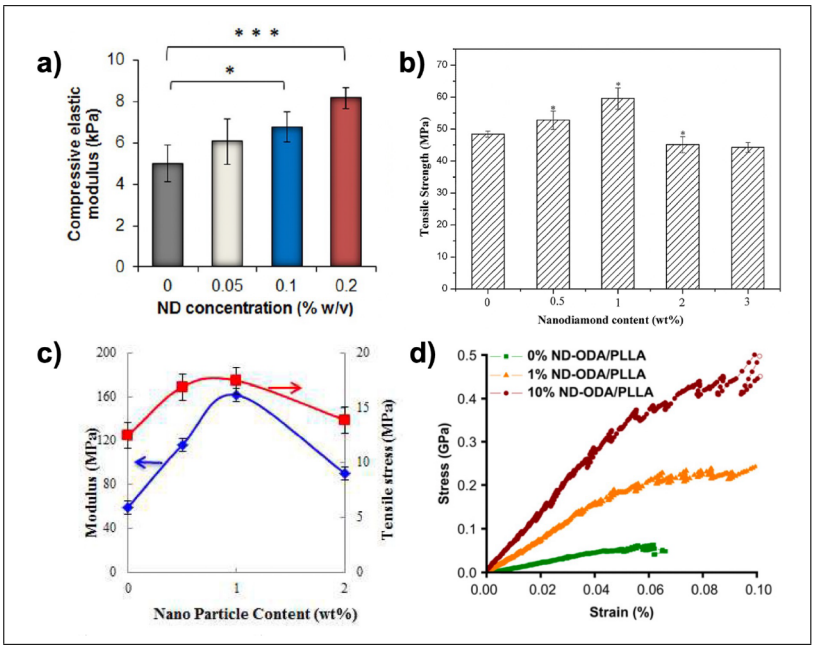

Figure 2.5 The effect of ND on a) compressive elastic modulus of gelatin methacrylamide [46] b) tensile strength of polyvinylidene fluoride [48] c) Young's modulus of polyurethane [57] and d) Young's modulus of PLLA [47].

As shown in Figure 2.5, the respective studies have demonstrated that the incorporation of ND enhances the tensile and compressive strength and Young's modulus of

the polymeric scaffolds. According to Zhang et al.[59], Pacelli et al.[46] and Alishiri et al.[57], the affinity of the polar groups between polymer and ND particles is the reason for contribution of ND to the respective mechanical properties of polymeric scaffolds. However, the optimization of ND concentration is essential since ND particles are prone to agglomerate at high concentration and agglomerated ND particles decrease the tensile and compressive strength of polymeric scaffolds. To illustrate, Shuai et al.[48] and Alishiri et al.[57] observed a reduction in tensile strength of polymeric scaffold when they increased the ND concentration to 2 wt% from 1 wt% according to Figure 2.3(b) and Figure 2.3(c), respectively. These authors explain this weakening as a result of possible ND agglomeration at concentration of 2 wt% [48, 57].

In vitro cytotoxicity studies have indicated that ND is a biocompatible material but the addition of ND particles to polymeric scaffolds does not significantly enhance cell proliferation or osteogenic differentiation [45, 48, 51, 57]. However, ND was found to enhance the effect of osteogenic agents such as dexamethasone [46] and BMP-2 [50] when it was used in this scaffold with these agents. In the study conducted of Pacelli et al. [46], the incorporation of ND in gelatin methacrylate/dexamethasone was found to enhance the Ca mineralization and ALP activity. Moreover, Suliman et al. [50] demonstrated that ND boosted the impact of BMP-2 on ALP and COL1α expression. Overall, ND is a potential candidate to enhance compressive strength and modulus of CMC/Gel-incorporated CPCs without compromising the in vitro cell response.

2.5.2 Fullerenol

ROS such as superoxides are biological oxidants with high reactivity against DNA, RNA, lipids, and proteins. They occur as a result of cell communication and inflammation in the body. Research conducted with MSCs has shown that when ROS levels are optimal, they play a role in Wnt, Hedgehog, and forkhead transcription factor signaling pathways for MSC differentiation [60, 61].

Inflammation after implantation can cause high ROS levels [62]. Inflammation

caused by the bone scaffold is expected to be under control and resolved as soon as possible. The prolongation of the inflammation process leads to oxidative stress [60, 61] and slows down tissue healing [63].

Previous studies have revealed that increased levels of ROS trigger the apoptosis of osteoblasts, osteocytes, mesenchymal stem cells, and pre-osteoblast cells such as MC3T3-E1 cells [64, 65, 66]. Moreover, studies conducted so far have shown that oxidative stress accelerates the adipogenic and osteoclastic differentiation of MSCs while slowing down osteogenic differentiation [60, 67, 68]. Figure 2.6 schematically illustrates the effect of ROS on osteogenesis and adipogenesis by indicating the proteins that play a role in each differentiation.

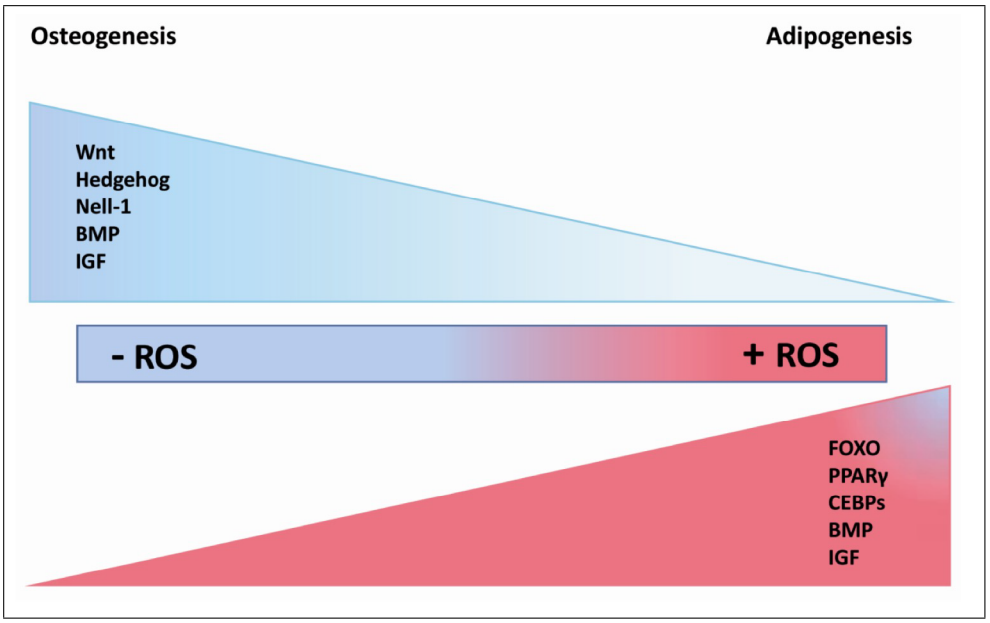

Figure 2.6 The effect of ROS on osteogenesis and adipogenesis of MSCs [60].

Antioxidants such as Trolox and selenium can promote cellular osteogenic differentiation via minimizing oxidative stress in cells [67, 68]. These antioxidants have also proven to be effective ROS scavengers when incorporated into brushite CPCs [61, 69]; however, their impact on osteogenic differentiation when used with these cements has not been assessed. Thus, the potential of antioxidants to enhance the osteogenic capability of CPCs remains unclear.

An advanced carbon nanomaterial, fullerene, is an antioxidant. Nevertheless, the utility of fullerene in biomedical applications is constrained by its insolubility in water. To overcome this, a functionalized fullerene with hydroxyls, fullerenol (Ful), has been extensively studied due to its solubility in water. Figure 2.7 presents fullerene and Ful's chemical structures.

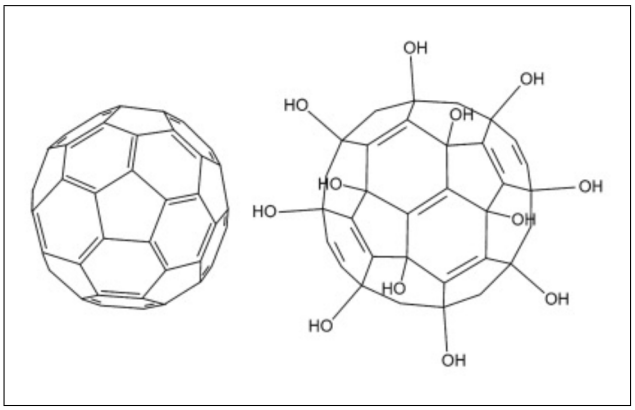

Figure 2.7 Fullerene (left) and Ful (right) [70].

The electron-deficient sites on Ful's surface are capable of efficiently transferring unpaired electrons of ROS molecules into the fullerene cage, thereby neutralizing them [71, 72]. According to Podolsky et al.[73], the presence of hydroxyl groups on Ful (molecular composition of $C_{60}(OH)_{22-24}$) further enhances its ROS scavenging capability, making it a more potent antioxidant than unmodified fullerene. Ful is also characterized by low cytotoxicity [74, 75].

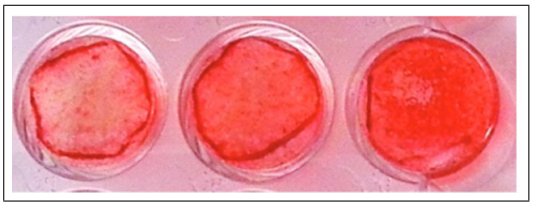

Figure 2.8 Osteogenic media with no Ful (left), 0.1 μM Ful (middle) and 1 μM Ful (right) after Alizarin Red staining [74].

The results shown in Figure 2.8 point out that the intensity of red color increased via increasing Ful concentration, which means the enhanced mineralization of stem cells with Ful [74]. Other research has highlighted Ful's ability to stimulate Runx2, alkaline phosphatase (ALP) and OCN [74, 76]. Therefore, Ful has the potential to improve the osteogenic characteristics of CMC/Gel-incorporated CPCs.

Finally, the studies investigating the interactions, ROS scavenging ability, cytotoxicity and osteogenic ability of Ful are summarized in Figure 2.9 by indicating the studied Ful concentration range [75, 77, 78, 79, 80].

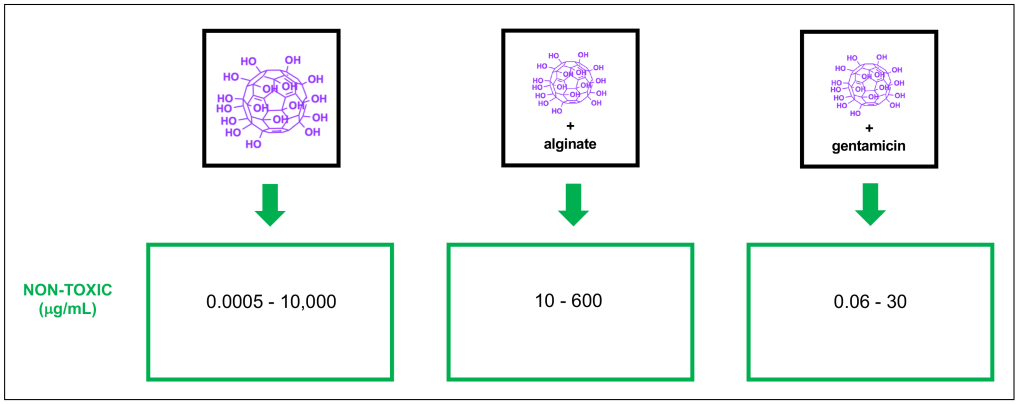

Figure 2.9 Non-toxic concentrations of Ful in bare and conjugated forms (Gentamicin concentration changed accordingly due to its conjugation to Ful)[75, 77, 78, 79, 80].

3. OPTIMIZATION OF POWDER AND LIQUID PHASES OF CEMENTS

This section includes the effort to optimize the powder and liquid phase of apatite cements to obtain appropriate setting time. For this purpose, first, pH and concentration of hardening agent solution were investigated. Second, the effect of cementing powder type and size was studied Finally, setting time analysis was accomplished on cements composed of different powder and liquid phases via Gilmore test.

3.1 Experimental Procedure

3.1.1 Preparation of Liquid Phase

A hardening agent solution was used as liquid phase of cements. 0.4 M hardening agent solution with a pH of 9.3 was prepared via dissolving 5.68 wt/v% Na_2HPO_4 in distilled water. pH of the solution was decreased from 9.3 to 7.4 via dropwise titration with 1 M HCl to prepare liquid phase with 7.4.

3.1.2 Preparation of Cements from TTCP, DCPD and $CaSO_4$

TTCP/DCPD powder was prepared via mixing DCPD and TTCP in equivalent masses was ground and sieved through a 75 μm sieve. To prepare TTCP/DCPD/$CaSO_4$ powder, the sieved TTCP/DCPD was mixed with $CaSO_4$ powder sieved through a 75 μm sieve in the weight ratio of 1/1/2. Different cements were prepared via mixing TTCP/DCPD and TTCP/DCPD/$CaSO_4$ powders with liquid phases with different pH values of 7.4 and 9.3.

3.1.3 Ball Milling of TTCP/DCPD Powder and Characterization of Powder

The sieved powder mixture of TTCP and DCPD was ball-milled in absolute ethanol with 3 mm yttria stabilized zirconia balls at 120 rpm [31, 81]. Absolute ethanol was chosen to keep the powder mixture un-dissolved and 120 rpm was selected from calculating 75% of critical speed [82]. The weight ratio of powder/ethanol/ball was 1/2/1.30. Following the ball milling process, the slurry was subjected to drying at 50 $^{\circ}C$ and grounded into powder.

The TTCP/DCPD powder was characterized via SEM and XRD before and after ball milling process. SEM images of particles were obtained in secondary electron mode with a Philips-FEI XL30 and the average particle size was measured via ImageJ. Finally, XRD spectra were taken using a Rigaku D/MAX-Ultima+/PC equipped with CuKα radiation and step angle of 0.02.

3.1.4 Preparation of Cements from Ball-milled TTCP/DCPD Powder

The ball-milled TTCP/DCPD powder was combined with a liquid phase having a pH of 7.4.

3.1.5 Setting Time Analysis

Setting time analysis was conducted by the Gilmore test according to standard C266-20 from the American Society for Testing and Materials [83] for the cements prepared from different powders and liquid phases with different pH values. Respective specimens were fabricated at 5 mm height and 10 mm diameter, immersed in phosphate buffered saline (PBS) and kept at 100% relative humidity at 37 $^{\circ}C$. The final setting times were assessed using a Gilmore apparatus (Utest) by recording the time at which heavy needle (d = 1.06 ± 0.05 mm, m= 453.6 ± 0.5 g) could not make an indentation

in the respective sample.

3.2 Experimental Results

3.2.1 Effect of Powder Material and pH

Table 3.1 shows if an indentation was observed after the cement hardening for 2 hours.

Table 3.1
Effect of powder material and pH on final setting time.

	pH:9.3	pH:7.4
TTCP/DCPD/$CaSO_4$	Indentation	Indentation (Slightly harder sample)
TTCP/DCPD	No indentation	No indentation (Slightly harder sample)

Gilmore test results show that powder material and pH both affect the setting time. According to the results, removing $CaSO_4$ from the powder formula and decreasing pH of the liquid phase were efficient to decrease the setting time. However, the setting time was still above 1 hour.

3.2.2 Effect of Particle Size

Figure 3.1 demonstrates the particle size and crystallinity after ball milling.

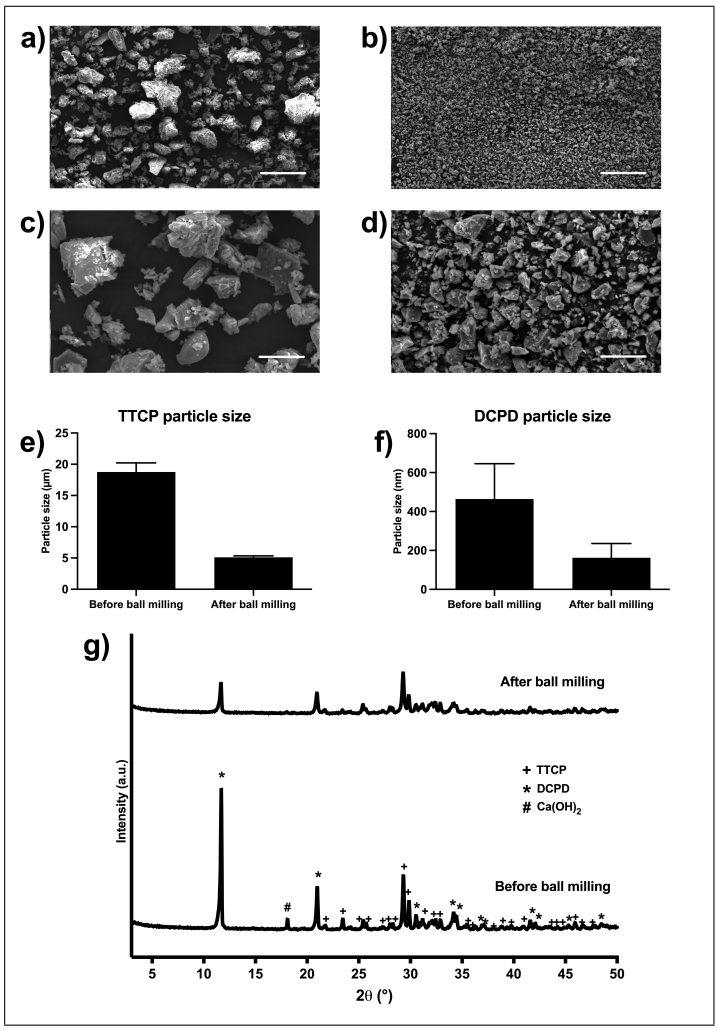

Figure 3.1 (a) SEM image of TTCP/DCPD particles before ball milling (Scale bar=50 μm) (b) SEM image of TTCP/DCPD particles after ball milling (Scale bar=50 μm) (c) SEM image of TTCP/DCPD particles before ball milling with higher magnification (Scale bar=10 μm) (d) SEM image of TTCP/DCPD particles after ball milling with higher magnification (Scale bar=10 μm) (e) Change of TTCP particle size via ball milling (f) Change of DCPD particle size via ball milling (g) XRD spectrums of TTCP/DCPD particles before and after ball milling.

Figure 3.1(a-b) show that smaller particle sizes in a narrower range were obtained via ball milling. The shapes of TTCP and DCPD can be seen in Figure 3.1(c-d); TTCP particles have round edges and smooth surfaces due to their sintering procedure, while DCPD particles are smaller, irregularly shaped, and adhered to the larger TTCP [94]. Figure 3.1(e-f) demonstrate the ImageJ analysis. According to ImageJ analysis, the average size of TTCP and DCPD particles were reduced from 18.8 μm and 464 nm to 5.1 μm and 162 nm via ball milling, respectively. In Figure 1g, XRD spectra taken before and after ball milling indicate that only DCPD and TTCP phases were present after ball milling.

Table 3.2 shows the initial and final setting times before and after ball milling.

Table 3.2
Effect of particle size on final setting time.

	Final setting time (min)
Before ball milling	>60
After ball milling	14

The final setting time reduced to 14 minutes after ball milling.

3.3 Discussion

For using cements in orthopedic applications, it is recommended to employ cements with an initial setting time of 8 minutes and a final setting time of 15 minutes [3]. The final setting time of cement consisted of calcium sulphate, tetracalcium phosphate (TTCP) and dicalcium phosphate dihydrate (DCPD) was observed more than 2 hours (Table 3.1). The primary reason for this result could be the presence of calcium sulphate since Song et al. [84] reported that $CaSO_4$ did not undergo hydration reaction to produce apatite. Therefore, calcium sulphate was reduced from the cement formula. After the reduction of calcium sulphate from cement formula, the final setting time was still found more than one hour and adjustments to particle size and pH reduced the final setting time to the recommended range (Tables 3.1 and 3.2). Efficiency of these adjustments is based on the enhancement of the particle solubility via reducing the particle size and pH and therefore, increasing the reactivity [29].

3.4 Conclusion

In conclusion of the optimization section of this thesis, final setting time of apatite cements was successfully adjusted to below fifteen minutes which is the recommended range for utility of CPCs in orthopedic applications. To do so, the reactivity of TTCP and DCPD was enhanced via increasing the solubility of TTCP and DCPD particles in the liquid phase. For increasing the solubility of these particles, particle size was reduced via ball milling and pH of the liquid phase was decreased to 7.4 via addition of 1 M HCl. Finally, the cement with adjusted particle size and pH was used in further studies as control cement to investigate the impact of polymers and carbon nanomaterials on physical and biological properties of CPCs.

4. NANODIAMOND-INCORPORATED CALCIUM PHOSPHATE CEMENTS

4.1 Experimental Procedure

4.1.1 Preparation of Cements

The composition of cements is showed in Table 4.1.

Table 4.1
The composition of ND-containing cements.

	Liquid phase (wt/v%)			Powder/Liquid (wt/wt)
	CMC	Gel	ND	
Control	0	0	0	1.25
CMC/Gel	1	0.5	0	1.25
ND0.01	1	0.5	0.01	1.25
ND0.02	1	0.5	0.02	1.25
ND0.04	1	0.5	0.04	1.25

Powder phase, hardening agent solution and control cement were prepared as explained in Section 3.1. For preparation of CMC/Gel solution, first, 0.5 wt/v% Gel from bovine skin (Sigma-Aldrich, United States) was dissolved in hardening agent solution for 15 minutes at 60 $^{\circ}C$. Then, 1 wt/v% CMC (Sigma-Aldrich, United States) was dissolved in the Gel solution at 90 $^{\circ}C$. After CMC/Gel solution was cooled at room temperature, CMC/Gel cements were prepared via mixing CMC/Gel solution with powder as previously described [10, 85]. ND0.01, ND0.02 and ND0.04 solutions were prepared via dissolving 0.01, 0.02 and 0.04 wt/v% ND particles in CMC/Gel solution via homogenizator, respectively. Gum-like consistency was obtained by using a powder/liquid weight ratio of 1.25 in all cements.

4.1.2 Setting Time Analysis

Cement samples' setting time were measured by the Gilmore test as indicated in Section 3.1.

4.1.3 Phase Analysis and pH Measurements

Samples were sunk in PBS solution and kept at a temperature of 37 $^{\circ}C$ for varying durations of 1, 3, and 24 hours. After each respective duration, the samples were extracted from the PBS solution and frozen at a temperature of -80 $^{\circ}C$. Subsequently, they were lyophilized for 24 hours before being analyzed via XRD. The XRD spectra were obtained at 2θ=20-50° using CuKα radiation on a Rigaku D/MAX-Ultima+/PC instrument. The step angle used was 0.02° [86].

To measure the pH of the cements, cement samples were subjected to incubation at 37 $^{\circ}C$ in PBS solution. The pH of PBS was measured at specific intervals between 1 hour and 28 days using a pH meter (MP225, Mettler Toledo). The PBS solution was replaced every 2 days [86].

4.1.4 Compression Test

To conduct the compression test, the cements were shaped into cylindrical specimens with a diameter of 10 mm and a length of 20 mm. Prior to testing, the cements were kept in PBS at a temperature of 37 $^{\circ}C$ for 24 hours and their height and diameter measurements were confirmed. The compression test was conducted on wet specimens using a Zwick roell z100 testing system, which featured a load cell of 100 kN and a crosshead speed of 0.5 mm/min [12]. The compressive modulus and strength values were obtained by analyzing the processed stress/strain data.

4.2 Results

Figure 4.1 demonstrates the setting time of cements.

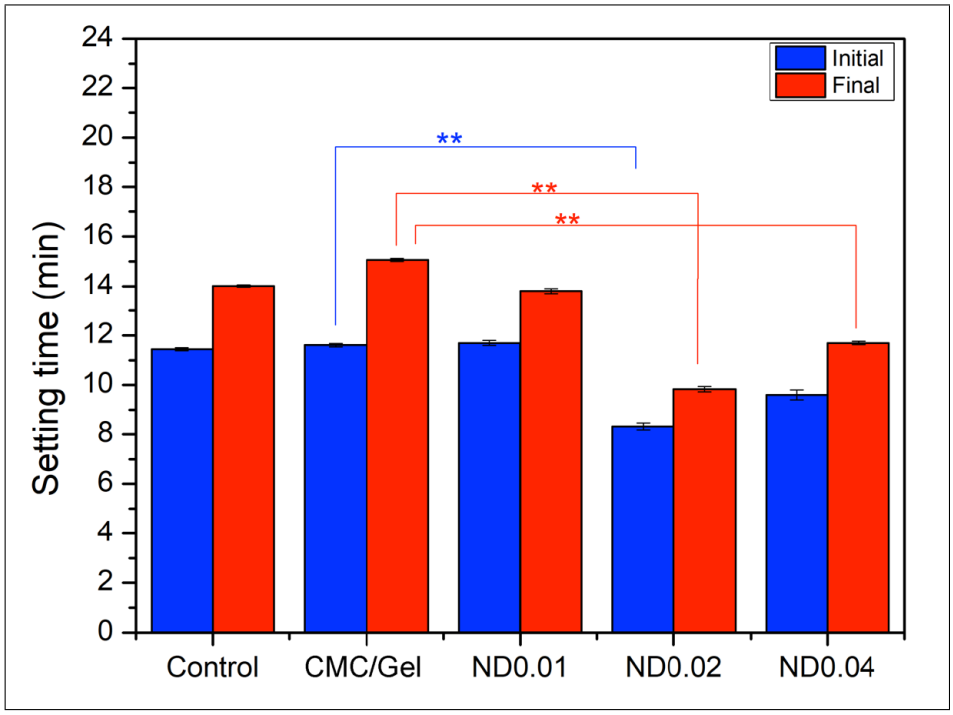

Figure 4.1 Initial and final setting times of ND-containing cements (n=5), mean±SEM, *=p<0.05, **=p<0.01).

The data in Figure 4.1 indicates that the addition of 1 wt/v% CMC and 0.5 wt/v% Gel did not have a significant impact on the setting time of the control cement. In addition, the inclusion of 0.01 wt/v% ND did not noticeably alter the setting time of CMC/Gel. However, the incorporation of 0.02 wt/v% ND resulted in a significant decrease in both the initial and final setting time of CMC/Gel cement, reducing the times to 8.3 and 9.8 minutes from 11.6 and 15.1 minutes, respectively. Further incorporation of ND did not significantly change the initial and final setting.

Figure 4.2 presents the apatite formation rate of ND-containing cements via XRD and pH analysis.

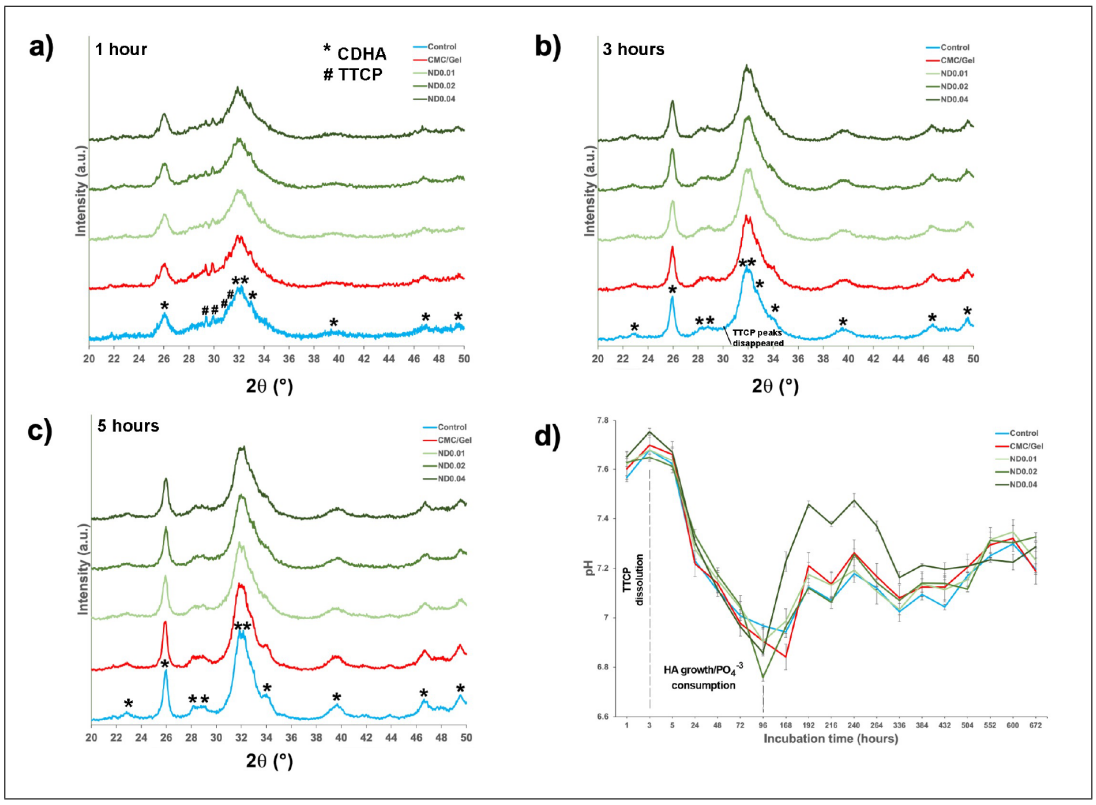

Figure 4.2 (a) XRD patterns of ND-containing cements incubated in PBS for 1 hour, (b) 3 hours, and (c) 24 hours. (d) pH changes of cement-incubated PBS over 672 hours (n=5).

According to the XRD spectra displayed in Figure 4.2(a-c), apatite formation began in less than an hour for all cements, completely consuming the DCPD. The residual amounts of TTCP were still present at the one-hour mark and it was subsequently consumed within 3 hours, resulting in the formation of apatite, as shown in Figure 4.2(b). This conversion was further supported by the increased height of the apatite peaks between 1 and 24 hours (Figure 4.2(a-c)). The incorporation of ND into the cements did not affect the time required for the conversion of TTCP and DCPD to CDHA, as depicted in XRD spectra.

The pH changes depicted in Figure 4.2(d) confirms the TTCP/DCPD conversion kinetics observed in the XRD analyses. In the first 3 hours, the pH of all solutions increased but subsequently decreased significantly due to the absence of basic TTCP, consumption of phosphate from the physiological solution, and subsequent growth of apatite [29, 87]. The control and CMC/Gel cements reached their minimum pH at day 7, while the ND0.01, ND0.02 and ND0.04, possibly due to the greater amount

of functional groups from the ND, which can serve as nucleation sites for Ca^{+2} ions [34, 88]. The minimum pH level for all cement solutions ranged from 6.7 to 7.0, and after reaching the minimum, the pH increased and remained constant between 7.0 and 7.4.

Figure 4.3 demonstrates the apatite morphology in cements.

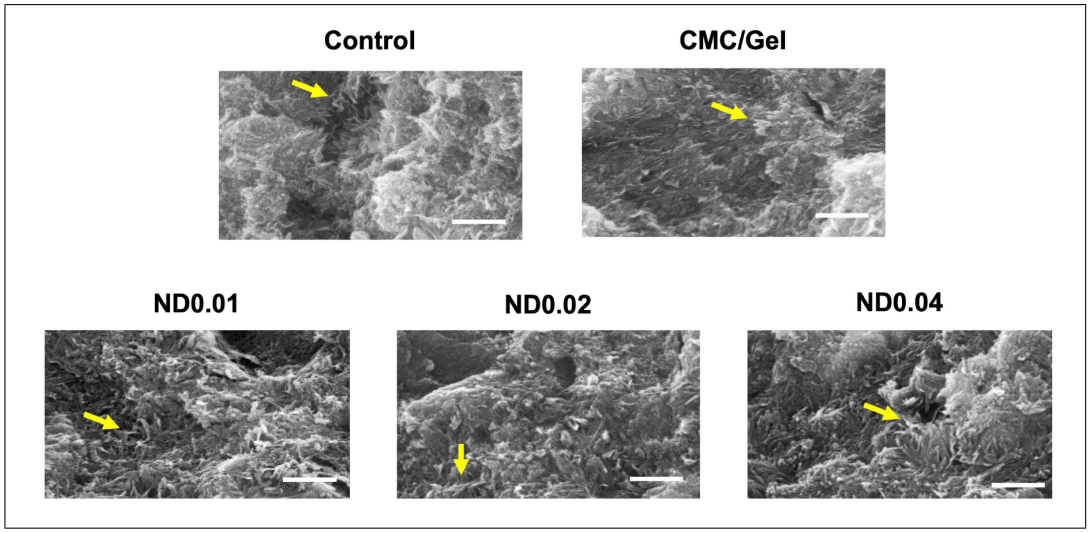

Figure 4.3 Apatite morphology in ND-incorporated cements immersed in PBS (Scale bars=500 nm, yellow arrows: apatite crystals).

As shown in Figure 4.3, the apatite morphology in all cements was nanosized platelet-like morphology [89, 90] and apatite morphology was similar in all cement groups.

Figure 4.4 demonstrates the results of compression test.

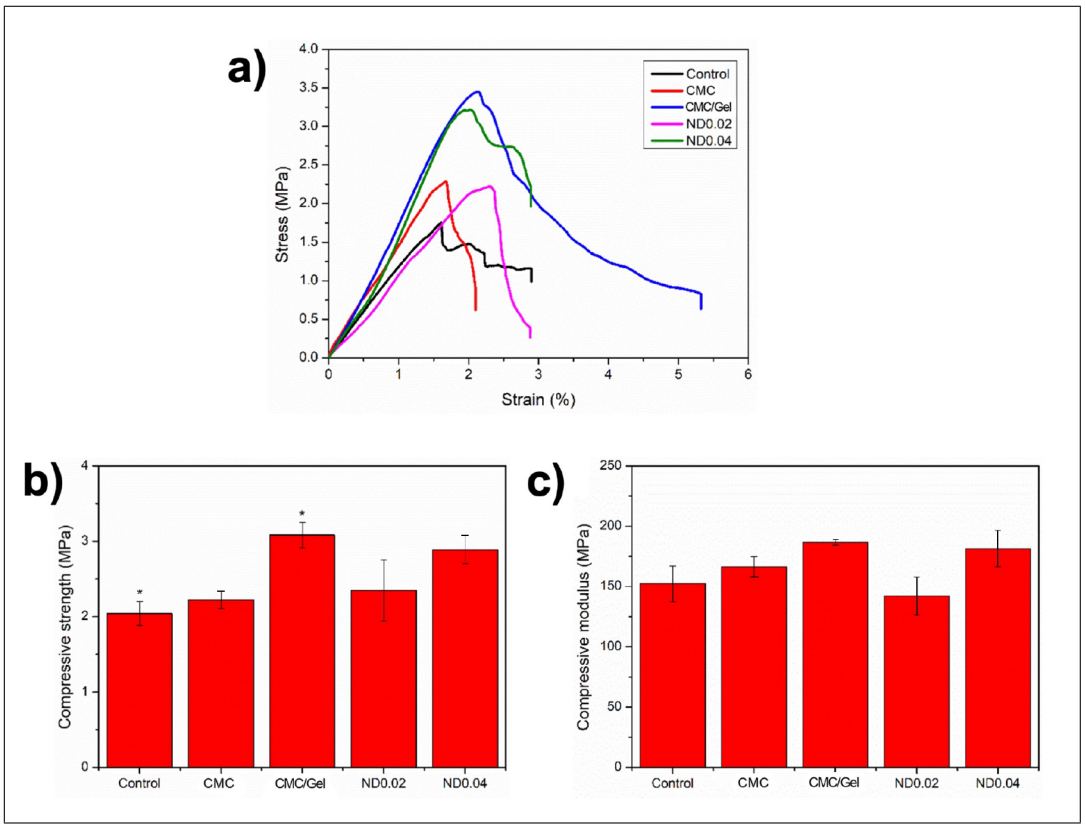

Figure 4.4 (a) Stress-strain graphs (b) Compressive strength and (c) Compressive modulus of ND-incorporated cements (n=5, * for $p<0.05$).

Figure 4.4 illustrates that the addition of 1 wt/v% CMC did not alter the compressive strength of the control cement. However, when 0.5 wt% Gel was incorporated into CMC cement, a significant increase in compressive strength from 2.22 MPa to 3.08 MPa was observed. On the other hand, the impact of Gel incorporation on compressive modulus was not found to be significant. Moreover, ND did not contribute to the compressive strength and modulus of CPCs.

4.3 Discussion

The baseline and CMC/Gel CPCs had an initial/final setting time in the range of 11/14 minutes (Figure 4.1). Interestingly, high concentrations of ND acted as a facilitator to reduce the setting time of CMC/Gel CPCs. Although the addition of 0.01 wt/v% ND did not alter the initial and final setting times of CMC/Gel cements, the inclusion of ND at higher concentrations significantly reduced the initial and final setting times, bringing the initial setting time closer to the clinically recommended time frames [3, 91] (Figure 4.1). The increased cement reactivity is possibly due to an increase in the common ion effect through the hydrogen bonding of functional groups on ND particles to HPO_4^{-2} [92]. Thus, these results indicate that HPO_4^{-2} sites on ND0.02 and ND0.04 facilitated the binding of Ca^{+2} ions, promoting apatite nucleation in these ND-doped cement formulations.

Although ND inclusion in CPC cements led to a decrease in their setting time, it did not have a significant impact on the conversion rate of TTCP and DCPD particles into CDHA domains, as shown in Figure 4.2. These materials showed only CDHA phase remaining after 3 hours (Figure 4.2(b)). The apatite formation rate from TTCP and DCPD was one of the fastest reported in the literature [93, 94, 95]. This rapid apatite formation could be attributed to the use of smaller-sized TTCP and DCPD particles and sodium phosphate solution instead of distilled water [29] (Table A-1).

Cancellous bone exhibits compressive strength values ranging from 2 to 16 MPa and compressive moduli in the range of 120-1100 MPa [17, 18] as shown in Table 2.1. Therefore, it is crucial to synthesize a CPC with similar mechanical properties to provide mechanical stability with cancellous bone implants [32, 96]. As per previous reports, the mechanical characterization data in Figure 4.4 demonstrate that the addition of CMC to the cements had no impact on compressive strength and modulus [4, 97], while Gel improved their compressive strength [6, 10, 98]. Although all formulations are fitting in the range of 2 MPa for strength and 150 MPa for modulus (Figure 4.4), ND incorporation did not impact the compressive strength and modulus of CMC/Gel samples, which is the main focus of this study.

First possible reason for the lack of contribution of ND on compressive strength are its potential to slow down the apatite reaction between TTCP and DCPD, and/or the agglomeration of ND [99, 96]. Since it has been observed that ND did not alter the apatite formation rate (Figure 4.2), aggregate formation is expected to be reason as mentioned in literature [48, 57]. It has not been possible to obtain a homogeneous liquid phase above a concentration of 0.02 wt/v%. The homogeneity of liquid phases containing ND up to this concentration destabilize quickly and can be the reason for having no effect on their mechanical properties. It is reported in the literature that more homogeneous ND solutions can be produced via functionalizing ND [57]. Future studies focusing on synthesizing homogeneous ND solutions are required to have a clear statement for the potential of ND for increasing the compressive strength of CPCs.

4.4 Conclusion

In this thesis, an apatite CPC from TTCP and DCPD was successfully synthesized. One of the fastest apatite formation rates in the literature was detected in this study. TTCP/DCPD conversion to apatite was found to complete in less than three hours.

To enhance the handling properties and compressive strength of cements, CMC and Gel were added in the liquid phase, respectively and CMC/Gel addition did not alter the apatite formation rate of the cements. For further improvement of the cements, carbon nanomaterials were incorporated into the cements. Unfunctionalized ND was incorporated to increase the compressive strength of the cements and Ful was used to enhance the osteogenic ability of the cements.

ND incorporation at high concentrations was found to decrease the setting time of CMC/Gel cements; however, the addition of ND did not compromise the apatite formation rate. Moreover, it was found that ND particles did not contribute to the compressive strength of the cements. This can be associated with the inhomogeneity of the liquid phases due to the ND aggregation. Hence, the collective data on ND particles point out that usage of unfunctionalized ND particles are efficient to decrease the setting time of the cements without compromising the total duration of apatite formation; however, aggregation of ND particles needs to be prevented to enhance the compressive strength of the cement.

5. FULLERENOL-INCORPORATED CALCIUM PHOSPHATE CEMENTS

5.1 Experimental Procedure

5.1.1 Preparation of Cements

The composition of cements is presented in Table 5.1.

Table 5.1
The composition of Ful-containing cements.

	Liquid phase (wt/v%)			Powder/Liquid (wt/wt)
	CMC	Gel	Ful	
Control	0	0	0	1.25
CMC/Gel	1	1.5	0	1.25
Ful0.02	1	1.5	0.02	1.25
Ful0.04	1	1.5	0.04	1.25
Ful0.1	1	1.5	0.1	1.25

Powder phase, hardening agent solution and control cement were prepared as explained in Section 3.1 and CMC/Gel solution was prepared as reported in Section 4.1.1 using the ratios indicated in 5.1. For preparation of Ful0.02, Ful0.04 and Ful0.1 solutions, 0.02, 0.04, or 0.1 wt/v% $C_{60}(OH)_n \cdot mH_2O$ Ful (n>40, m>8, Sigma-Aldrich, United States) were dissolved in CMC/Gel solutions, respectively. Ful handling and incorporation into the solutions was all done in fume hood or an enclosed glovebox. Gum-like consistency was obtained by using a powder/liquid weight ratio of 1.25 in all cements.

5.1.2 Structural Analysis

For analyzing the functional groups in the respective cements' liquid phases, Fourier Transform Infrared Spectroscopy (FTIR, Nicolet FTIR Instruments, Thermo Fisher Scientific) was used. Spectrum from 4000 cm^{-1} to 550 cm^{-1} was obtained with 32 scans [100].

5.1.3 Setting Time Measurements

Setting time of cement samples were measured by the Gilmore test as explained in Section 3.1.

5.1.4 Phase Analysis and pH Measurements in PBS

Phase analysis and pH measurements of Ful-incorporated cements were assessed as indicated in the Section 4.1.3.

5.1.5 Phase Analysis and pH Measurements in Simulated Body Fluid (SBF)

For the SBF preparation, the procedure outlined in Kokubo et al. [101] was followed. Then, the cements were incubated in SBF for durations of 3 hours and 24 hours. At these time intervals, the cements were retrieved from the incubator, separated from the SBF, and stored together with the as-prepared cements in a -80 $°C$ freezer. Subsequently, the cements underwent a 24-hour lyophilization process. XRD spectra of the cements were acquired using a Bruker D8 Advance XRD instrument. To monitor pH changes over time, the cements were immersed in SBF and pH measurements were taken at specific intervals ranging from 1 hour to 14 days using a pH meter (MP225, Mettler Toledo). The SBF solution was refreshed every 2 days.

5.1.6 Imaging of Apatite Formation

For imaging of surface morphology and apatite formation, cements were kept in PBS for 24 hours at 37 $°C$. After 24 hours, PBS was aspirated and samples were lyophilized. Lyophilized specimens were sputter coated with platinum, and cross-sectional images of fractured surfaces were obtained with a Philips-FEI XL30 SEM in 100x-100,000x magnification in secondary electron mode. This analysis was also carried out using simulated body fluid (SBF), following the protocol outlined in Kokubo et al. [101]. The samples were immersed in SBF for 24 hours at 37 $°C$. Additionally, cross-sectional images of the resulting cements were obtained using a Thermo Scientific Quatro S Environmental SEM in secondary electron mode, allowing for an image magnification of 160,000x via ETD detector without the requirement of sample sputter coating. Energy dispersive X-ray spectroscopy (EDX) was conducted on the same device using a GSED detector to determine cements' elemental Ca/P ratio.

5.1.7 Compression Test

Compression test was conducted as explained in the Section 4.1.4.

5.1.8 In vitro ROS Scavenging Ability Test

In vitro ROS scavenging ability of Ful containing cements and CMC/Gel were assessed using a 1,1-Diphenyl-2-picrylhydrazine (DPPH) assay [102, 103]. DPPH solutions were prepared by dissolving 31.62 mg DPPH (Sigma-Aldrich, United States) in 400 mL 80:20 v/v% solution of ethanol (Thermo Fisher Scientific, United States) and deionized water. 10 mg respective cement samples were immersed into 2 mL DPPH solution and shaken at 37 $°C$ in the dark. At 1, 12, and 24 hours, 100 μL samples of DPPH were removed and absorbance was measured on a Tecan MPlex microplate reader at 517 nm. Absorbance values of DPPH solutions incubated with Ful containing cements (A_{Ful}) were compared to absorbance readings of DPPH solution incubated

with CMC/Gel cement ($A_{CMC/Gel}$) as shown in Eq. 5.1 below.

$$\%\text{DPPH Amount} = (1-((A_{Ful} - A_{CMC/Gel})/A_{CMC/Gel}))\text{x}100 \quad (5.1)$$

5.1.9 In vitro Ful Release from CPCs

Ful particles were labeled with fluorescein 5-isothiocyanate (FITC, Thermo Fisher Scientific, United States) via an isothiocyanate-hydroxyl conjugation for determining the amount of Ful released from cements. First, 1 mg Ful was dissolved in 2 mL anhydrous dimethyl sulfoxide (Sigma, Germany). Then, 3 mg FITC was added into solution and stirred for 16 hours in the dark at room temperature. 13 mL acetone (Thermo Fisher Scientific, United States) was added to the reaction solution to precipitate out Ful-FITC while leaving unreacted FITC in the supernatant. The precipitated reaction mix was then spun down for 5 minutes at 3000xg and then the supernatant was removed and the remaining was air dried. As described above, cements were prepared with the Ful-FITC along with control and CMC/Gel cements.

30 mg cement samples were placed into individual wells in 24-well tissue culture plates containing 1 mL PBS. Then, plates were put on a shaker and kept in the dark. On days 1, 3, and 5, the fluorescence emissions of releaseate media were obtained at FITC's excitation wavelength at 495 nm and emission wavelength at 520 nm via microplate reader [104]. Fluorescence of pure PBS was subtracted from the releaseate readings. Finally, a standard curve was prepared from FITC solutions in serial dilutions of PBS and Ful-FITC release kinetics were determined using this curve.

5.1.10 In vitro Cell Culture Studies

Murine MC3T3-E1 pre-osteoblasts (Subclone 4, ATCC, United States) and murine L-929 fibroblasts (American Type Culture Collection (ATCC), United States) and murine were the two immortalized cell lines used for in vitro biological evalua-

tions. L-929s were cultured in Dulbecco's Modified Eagle's Medium low glucose (Gibco, United States) supplemented with 1% penicillin-streptomycin (Gibco, United States) and 10% fetal bovine serum (Gibco, United States). MC3T3-E1 cells were cultured in either growth medium (alpha-MEM without ascorbic acid (Gibco, United States), 10% fetal bovine serum, and 1% penicillin-streptomycin) or osteogenic medium (growth medium supplemented with 10^{-8} M dexamethasone (Thermo Fisher Scientific, United States), 50 mg.mL^{-1} β-glycerophosphate (Thermo Fisher Scientific, United States) and 0.01 mol.L^{-1} L-ascorbic acid (Thermo Fisher Scientific, United States). All cells were kept in a 95% humidified incubator with 5% CO_2 at 37 $^{\circ}C$.

5.1.10.1 In vitro Cytotoxicity Evaluation. A cytotoxicity test was performed according to ISO 10993-5 [105]. 30 mg cement samples were immersed in sterile PBS (1 mL, Sigma-Aldrich, United States), and the extracts were taken on days 1, 3, and 5. Then, the extracts were sterile filtered through 0.22 μm polyvinylidene fluoride (PVDF) hydrophilic membranes and mixed with growth medium in a 1:10 ratio.

When cultured L-929 cells reached confluency, they were seeded in a 96-well plate at a concentration of $5x10^3$ cells/well [106]. After overnight incubation, old media were removed, and cells were treated with 100 μL PBS with or without the respective cement extracts for 24 hours. MTS assay (Promega, United States) was conducted to determined metabolic activity. The absorbances were measured at 490 nm by using a microplate reader (Varioskan Lux, Thermo Fisher Scientific). The results were normalized to the absorbances of non-treated group.

5.1.10.2 Live-Dead Staining. Live-dead staining was conducted on the cells treated with day 3 cement extracts. First, the staining solution was prepared by adding 0.5 μL calcein (Thermo Fisher Scientific, United States) and 2 μL ethidium bromide (Thermo Fisher Scientific, United States) to 1 ml D-PBS (Gibco, United States). Then, the media on the cells was aspirated, cells were rinsed with D-PBS, and each well was treated with staining solution before incubating at 37 $^{\circ}C$ for 45 minutes. Finally, the

images were taken via fluorescence microscopy using FITC and Texas Red imaging channels (Axiovert A1, Zeiss) [107].

5.1.10.3 Cell Viability Test with Ful Particles. MC3T3-E1 cells were cultured to confluency and seeded in a 96-well plate at a density of 5,000 cells/well for 24 hours. Then, the cells were treated with 100 μL Ful in growth media in serial dilutions including 1000, 500, 250, 125, 62.5, and 0 μg/mL for 24 hours [75]. Finally, the solutions in each well were removed, and the CellTiterGlo (Promega, United States) solution was added. After incubation at room temperature for 10 minutes, the bioluminescence of the wells was measured at 515 nm by using a microplate reader (Tecan MPlex). Luminescence values for Ful-treated wells were normalized to the non-treated group.

5.1.11 In vitro Osteogenic Differentiation Studies

For osteogenic differentiation studies, cement formulations were incubated in growth medium for one week and extracts were collected [41]. The extracts were filtered through sterile 0.22 μm PVDF filters and combined with the osteoblastic induction medium in a 1:1 ratio to prepare the osteoblastic induction medium for each cement. Cells were cultured for 24 hours in growth medium. On the second day, half the medium in each well was aspirated before adding 1 mL of respective cement extract media samples. The osteogenic medium was refreshed every 2 or 3 days.

5.1.11.1 Immunofluorescence Staining. On day 7 post-treatment, cytoskeletal differences in treated MC3T3-E1 cells were examined. The culture medium was removed, cells were rinsed with PBS, and the cells were fixed with 3.7% formaldehyde (Riedel-De-Haën, Germany) at room temperature for 30 minutes. Cells were permeabilized with 0.1% Triton-X 100 (Biobasic, Canada) for 5 minutes before being incubated for 10 minutes in blocking solution. Cells were treated with Alexa Fluor 594 phalloidin

(Thermo Fisher Scientific, United States) for 60 minutes and cytoskeletal actin was imaged. Then, the samples were washed with PBS to remove unbound conjugates. Moreover, cell nuclei were stained with 4',6-diamidino-2-phenylindole (DAPI, Sigma, Germany) for 15 minutes. Finally, the samples were washed thoroughly with PBS before adding Prolong Diamond Antifade Mountant (Thermo Fisher Scientific, United States) and visualized under the fluorescence microscope (VertA1, Zeiss, Germany) using the DAPI and TRITC channels. Finally, the fluorescence intensity of actin was measured via ImageJ.

5.1.11.2 ALP Activity Test. For the ALP activity test, MC3T3-E1 cells were seeded in 6-well plates (2 mL media per well) at a density of 10,000 cells/cm^2 and cultured in osteogenic medium for either 7 or 14 days. At these time points, medium from the cells was first removed before briefly washing with D-PBS and trypsinizing. The trypsinized cells were taken to individual microcentrifuge tubes (1.5 mL) and lysed in cold D-PBS via vortexing. Lysates were processed to measure ALP activity according to the manufacturer's instructions (Abcam, United States). Briefly, the lysates were resuspended in 500 μL assay buffer and centrifuged at 16,000 rpm at 4 $^{\circ}C$ for 15 minutes. Supernatants were taken to a new tube and kept cold during the following steps.

To measure ALP activity, 80 μL supernatant samples were put into wells in 96-well tissue culture plates in serial dilutions and to each well, 50 μL p-nitrophenyl phosphate solution was added [108]. Subsequently, incubation was carried out in the dark for a duration of 60 minutes, followed by the addition of a 20 μl NaOH solution. The absorbance at 405 nm was then measured using a microplate reader (Tecan MPlex). The absorbance of the background was also measured and subtracted from the absorbance of the sample wells. Finally, the p-nitrophenol (pNP) concentration of each well was determined using the prepared standard curve, and ALP activity was calculated as shown in Eq. 5.2 below.

$$\text{ALP activity (U/mL)} = (\text{A/V})/\text{T} \qquad (5.2)$$

Where A is the amount of pNP generated in samples (μmol), V is the volume of sample (mL), T is the reaction time (minutes), and units are glycine units. A Bradford assay was also conducted to calculate protein amounts for normalizing ALP activity. Briefly, 250 μL Coomassie reagent (Bioworld, United States) was added to 5 μL supernatant and incubated at room temperature for 10 minutes. Finally, absorbance was measured at 595 nm with a microplate reader (Tecan MPlex), and protein amount was determined according to the prepared standard curve calculated with solutions of bovine serum albumin protein.

5.1.11.3 Polymerase chain reaction (PCR). MC3T3-E1 cells were seeded at 20,000 cells per well in a 12-well plate and incubated for 24 h to allow cells to adhere. Then, the cells were treated with 1 mL of a 1:1 volumetric mix of osteogenic medium and filtered extracts from respective cement formations. Cells were allowed to differentiate for 7 and 14 days and the media was replaced with fresh osteogenic media on days 4, 7, and 10. On days 7 and 14, cells were rinsed and lysed before extracting and purifying RNA using a PureLinkTM RNA Mini Kit (Invitrogen, Waltham, MA), according to the manufacturer's protocol. Extracted RNA was quantified using a NanoQuant plate on a Tecan MPlex microplate reader. Subsequently, cDNA was synthesized using an iScript Reverse Transcription Supermix for RT-qPCR (Bio-Rad, Hercules, CA). Quantitative real-time polymerase chain reaction (qRT-PCR) was conducted using iTaq Universal SYBRÂ® Green Supermix (Bio-Rad, Hercules, CA). Relative expression levels of Collagen Type 1 (COL1) and runt-related transcription factor 2 (RUNX2) were normalized to glyceraldehyde 3-phosphate dehydrogenase (GAPDH) with $\Delta\Delta$Ct method. Primer sequences are given in Table 5.2.

Table 5.2
Primer sequences used in qRT-PCR.

	Forward primer	Reverse primer
RUNX2	5'-CACTGGCGGTGCAACAAGA-3'	5'-TTTCATAACAGCGGAGGCATTTC-3'
COL1	5'-CCTGAGTCAGCAGATTGAGAACA-3'	5'-CCAGTACTCTCCGCTCTTCCA-3'
GAPDH	5'-GGTGAAGGTCGGTGTGAACG-3'	5'-CTCGCTCCTGGAAGATCGTG-3'

5.1.12 Statistical Analysis

All experiments employed at least n=3 samples per group unless otherwise stated. Results were reported as mean±standard error (SEM) and $p<0.05$ was considered statistically significant. Statistical analyses were conducted using IBM Statistics 25. Normality of data were determined via Shapiro-Wilk testing. For ALP activity on 14th day and setting time analysis, the significance of difference was calculated via Kruskal-Wallis with Dunn's test for pairwise comparisons. For the other analyses, one-way ANOVA followed by Tukey post-hoc testing was performed. GraphPad Prism 9 was used to plot the results and single asterisk (*), double asterisk (**), triple asterisk (***) and quadruple asterisk (****) were utilized to represent $p<0.05$, $p<0.01$, $p<0.001$ and $p<0.0001$ respectively.

5.2 Results

Figure 5.1 demonstrates FTIR spectra for the liquid phases of control, CMC/Gel, Ful0.02, Ful0.04, and Ful0.1 cements.

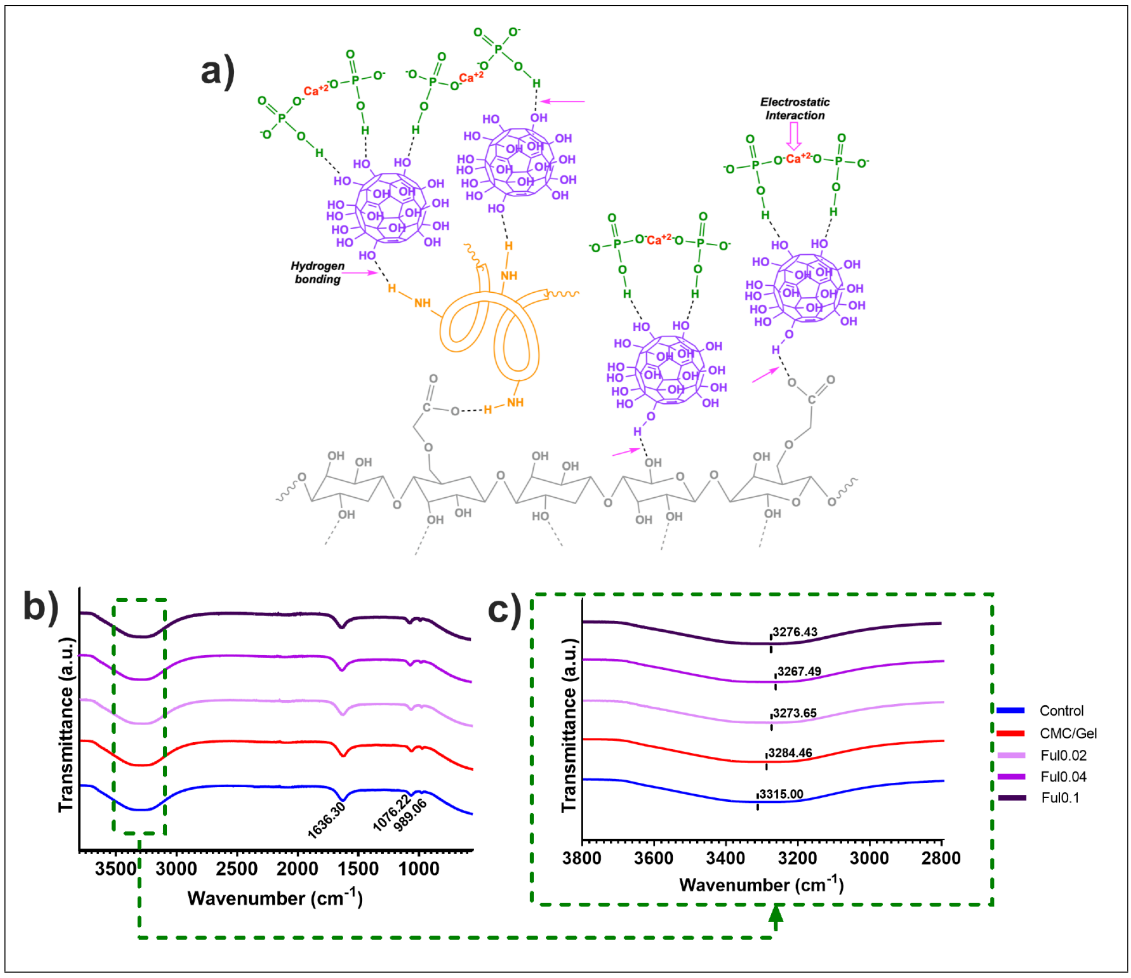

Figure 5.1 (a) Suggested structure and nucleation mechanism during cement hardening. (b) Total FTIR spectra of liquid phases. (c) Specific OH band between 2800 cm^{-1} and 3800 cm^{-1} in FTIR spectra of Ful-incorporated cements.

Figure 5.1(a) displays the proposed structure resulting from Ful conjugation to CMC/Gel cements. In Figure 1B, the FTIR spectrum of the control cement's liquid phase demonstrates characteristic peaks at 989.06, 1076.22, 1636.30, and 3315 cm^{-1}. These peaks correspond to the symmetric and asymmetric stretching vibrations of the P-O bond, bending vibration of the H-O-H bond, and stretching vibration of the OH bond, respectively [88, 109, 110]. Addition of CMC/Gel and/or Ful to the cement liquid phase caused a shift in the OH band as shown in Figure 5.1(c). The addition of

CMC/Gel caused the OH band at 3315.00 cm^{-1} to shift to a lower frequency of 3284.46 cm^{-1} due to stretching vibrations of OH groups in CMC and NH groups in Gel [111]. Incorporation of 0.02 and 0.04 wt/v% Ful to the cement liquid phases led to a further downshift to 3273.65 and 3267.49 cm^{-1}, respectively, due to an increase in OH content and hydrogen bonding in these samples [112, 113].

The results of the setting time measurements are illustrated in Figure 5.2.

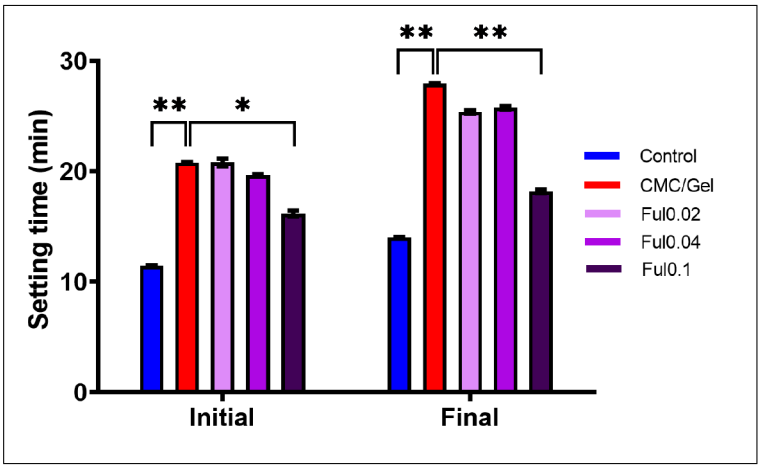

Figure 5.2 Initial and final setting times of Ful-incorporated cements (n=6, mean±SEM, *=p<0.05, **=p<0.01).

The results of setting time analysis show that the addition of CMC/Gel substantially increased both the initial and final setting times, from 11.4 and 14 minutes to 20.8 and 27.9 minutes, respectively. However, the inclusion of 0.02 and 0.04 wt/v% Ful did not cause any changes in the initial and final setting times of CMC/Gel. On the other hand, the addition of 0.1 wt/v% Ful resulted in a significant reduction in the initial setting time of CMC/Gel to 16.2 minutes and the final setting time to 18.2 minutes. These measurements suggest that the hardening of CMC/Gel cements was accelerated by 0.1 wt/v% Ful.

Figure 5.3 presents the apatite formation in the cements.

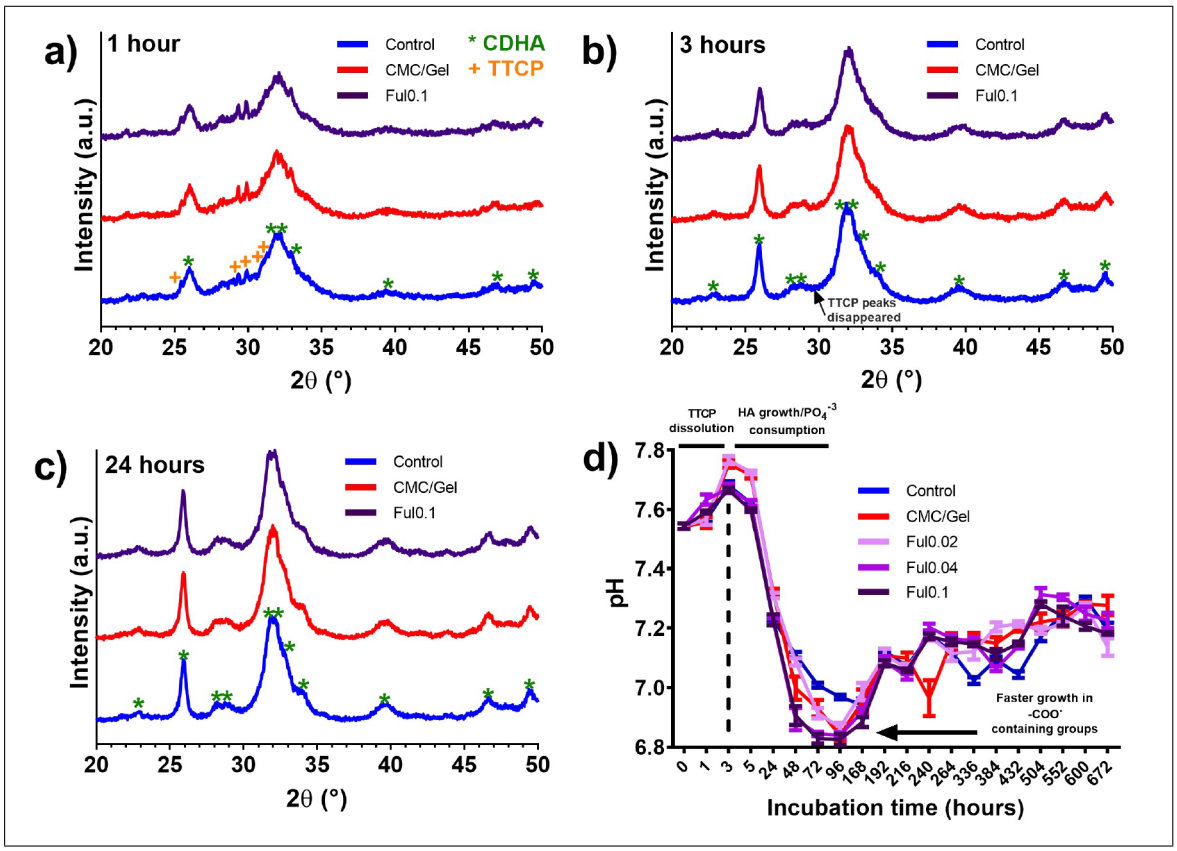

Figure 5.3 (a) XRD patterns of Ful-incorporated cements incubated in PBS for 1 hour, (b) 3 hours, and (c) 24 hours. (d) pH changes of cement-incubated PBS over 672 hours (n=5).

XRD spectra in Figure 5.3(a-c) illustrate the crystal phases of the cements under physiological conditions at hours 1, 3, and 24. The spectrums were similar to the spectrums depicted in 4.2(a-c) and apatite formation was observed in less than 3 hours. No Ful contribution to the apatite formation rate was detected. The graph showing pH measurements(Figure 5.3(d)) were also similar to the pH measurement presented in Fig 4.2(d) and confirmed the apatite formation kinetics as explained in the Section 4.2. Control cements reached their minimum pH at day 7, while CMC/Gel, Ful0.02, Ful0.04, and Ful0.1 cements reached their minimum pH at day 4, possibly due to the greater amount of $-COO^{-}$ ions from the CMC/Gel, which can act as nucleation sites for Ca^{+2} ions [34, 88]. The minimum pH level for all cement solutions was between 6.8 and 7.0, and after reaching the minimum, pH increased and remained constant between 7.0 and 7.4.

Figure 5.4 demonstrates the apatite morphology in the cements.

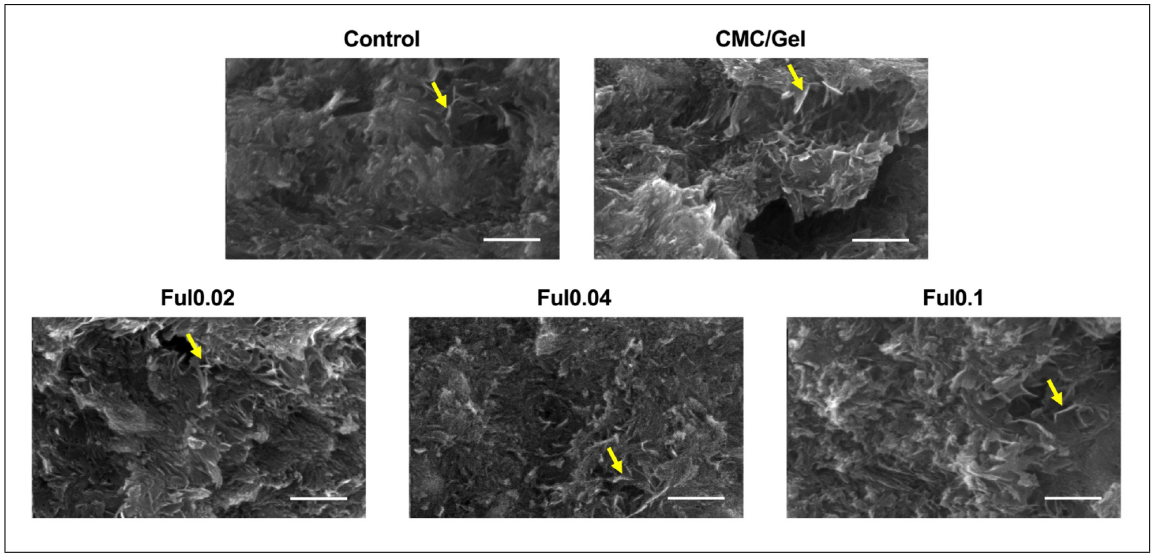

Figure 5.4 Apatite morphology in Ful-incorporated cements immersed in PBS (Scale bars: 500 nm, yellow arrows: apatite crystals).

Apatite morphology was nanosized platelet-like morphology [89, 90], with no obvious differences between five cement groups.

In addition to PBS, phase analysis of cements was conducted by incubating them in SBF and comparing them with the original cements. The results are presented in Figure 5.5.

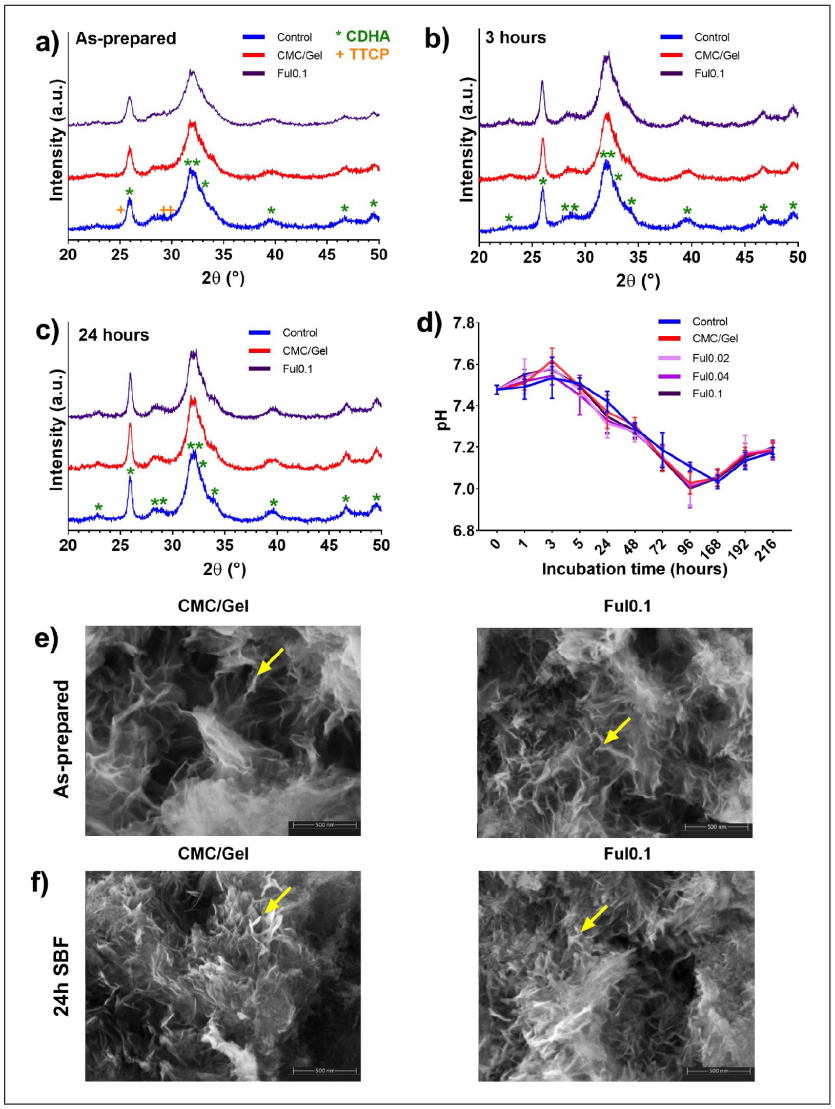

Figure 5.5 (a) XRD patterns of as-prepared cements before incubation, or (b) cements incubated in SBF for 3 hours and (c) 24 hours. (d) pH changes of cements incubated in SBF over 216 hours (n=5). (e) SEM micrographs showing the apatite morphology in as-prepared cements and (f) SBF-incubated cements for 24 hours (Magnification= 160,000x, yellow arrows: apatite cystals).

The XRD spectrum of the original cements (Figure 5.5(a)) reveals a significant presence of apatite in their crystalline phase even without SBF incubation. Moreover, XRD spectrums of incubated cements shows that conversion of TTCP/DCPD to apatite is complete in less than 3 hours and increasing the intensity of apatite peaks in 24 hours (Figure 5.5(b-c). Additionally, the pH change of SBF-incubated cements over time (Figure 5.5(d)) exhibited a similar pattern to the pH profile in PBS (Figure 5.4(d)). Finally, SEM images of the cements before incubation in SBF (Figure 5.5(e)) and after SBF treatment (Figure 5.5(f)) reveal the presence of nanosized platelet-like

crystals [89, 90], indicating apatite formation. Importantly, the as-prepared cements (Figure 5.5(e)) did not show noticeable differences between the materials incubated in PBS (Figure 5.4) or SBF (Figure 5.5(f)).

EDX results showing the Ca/P ratio after incubation in SBF for 24 hours are presented in Figure 5.6.

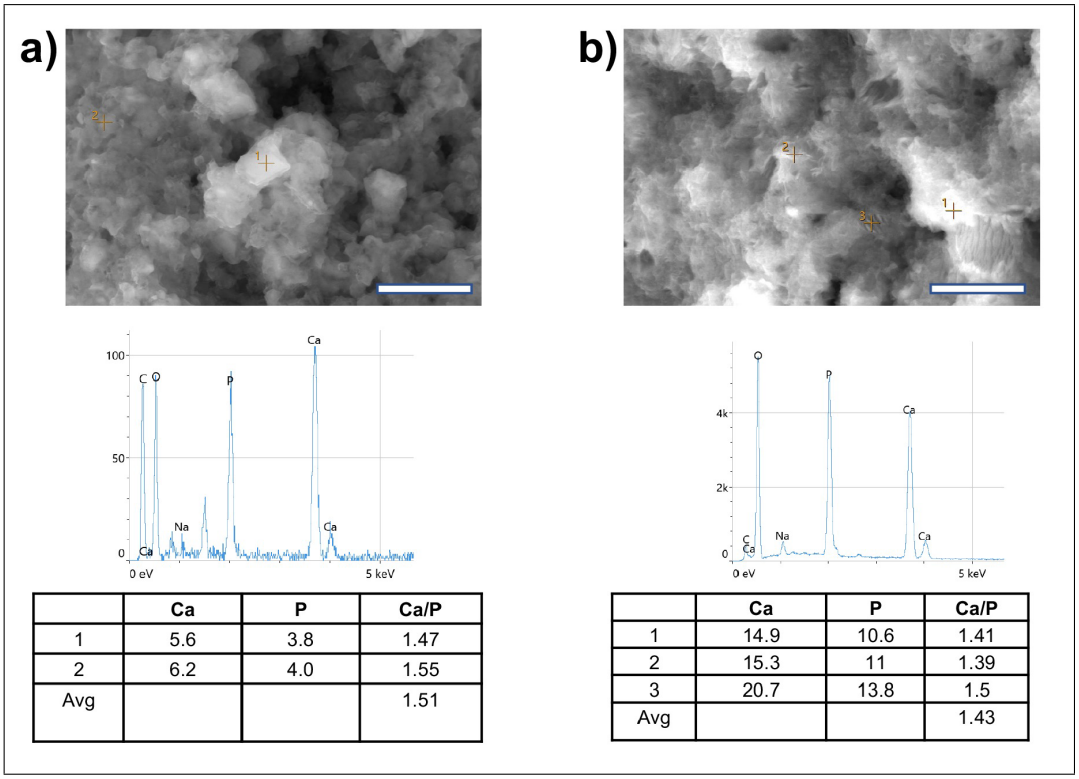

	Ca	P	Ca/P
1	5.6	3.8	1.47
2	6.2	4.0	1.55
Avg			1.51

	Ca	P	Ca/P
1	14.9	10.6	1.41
2	15.3	11	1.39
3	20.7	13.8	1.5
Avg			1.43

Figure 5.6 EDX analysis of a) CMC/Gel cements and b) Ful0.1 cements after incubation in SBF for 24 hours (Scale bars: 5 μm).

The incubated cements exhibited Ca/P ratios of 1.40-1.50. This represents the Ca/P ratio of CDHA [114] and confirms the CDHA formation in cements.

Figure 5.7 displays the results of mechanical testing conducted on CMC/Gel, Ful0.02, Ful0.04, and Ful0.1 cement formulations (shown as model samples in Figure 5.6(a)) through compression testing.

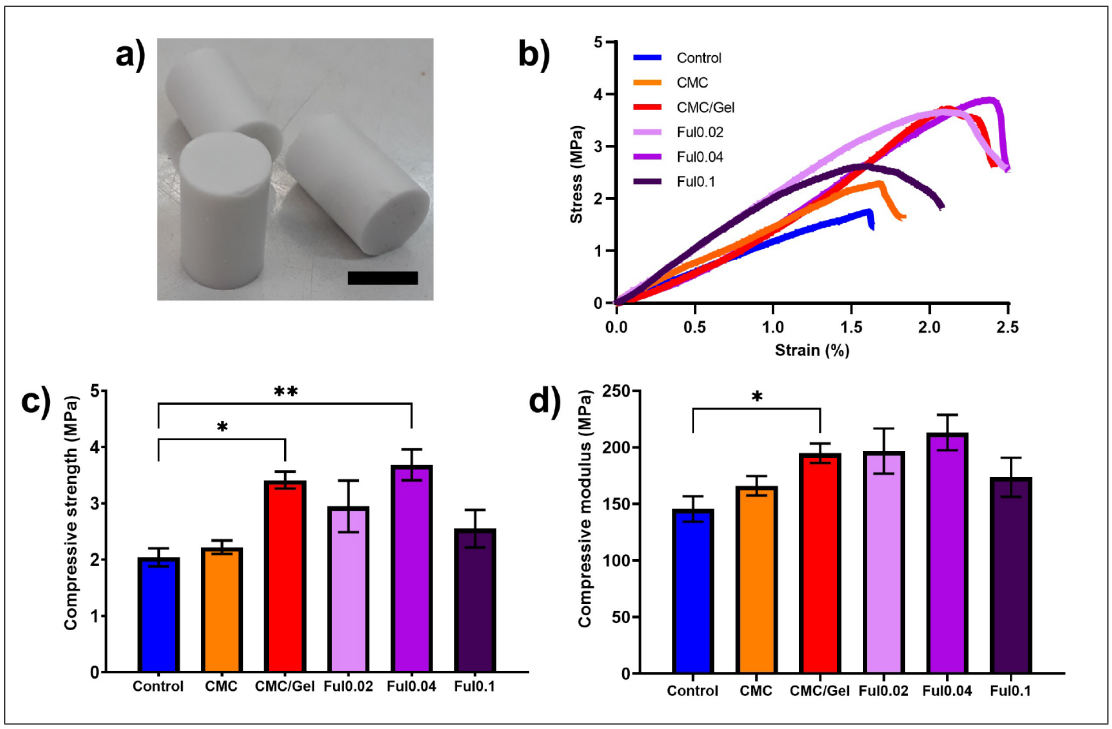

Figure 5.7 Mechanical analysis of Ful-incorporated cements (a) Photograph of cements molded for compression testing (Scale bar= 1.25 cm) (b) Representative stress-strain curves. (c) Compressive strength and (d) compressive modulus values of cements (n=5, * for $p<0.05$, ** for $p<0.01$).

Representative stress/strain curves are shown in Figure 5.7(b). The compressive strength and elastic modulus values of control cements were found to be 2.04 MPa and 145.55 MPa, respectively, as demonstrated in Figure 5.7(c-d). The addition of only CMC did not have a significant impact on the compressive strength or modulus when compared to unmodified control cement samples. However, CMC/Gel led to a significant increase in compressive strength and modulus in comparison to control samples. Lastly, the inclusion of Ful did not produce any significant changes in the compressive strength and modulus values of CMC/Gel formulations.

A DPPH radical inhibition assay was conducted on cement samples to evaluate the antioxidant capacity of Ful-loaded CPCs and the results are shown in Figure 5.8.

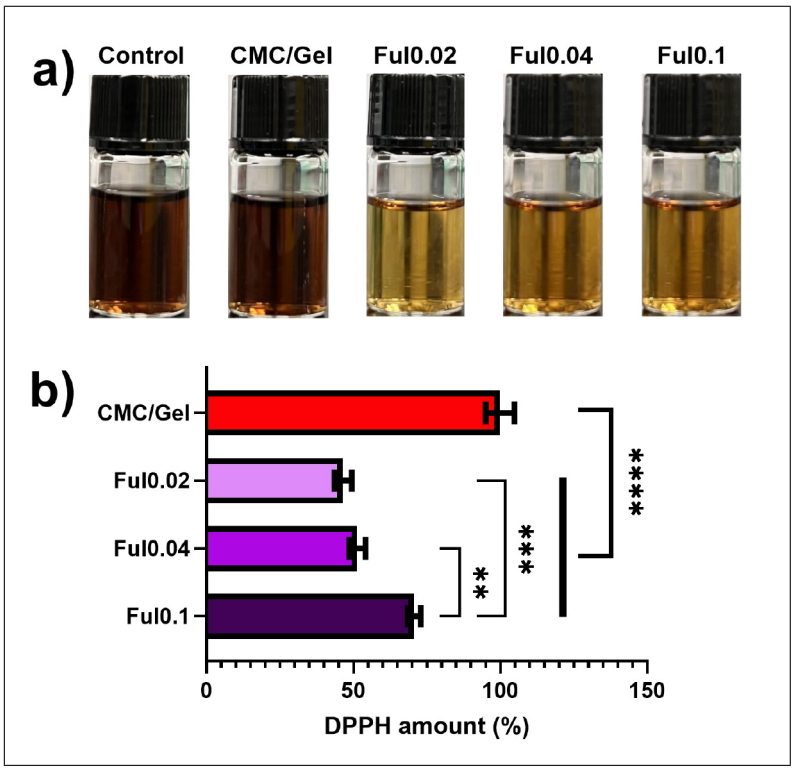

Figure 5.8 (a) Digital photos of DPPH solutions after 24-hour-treatment with cements. (b) DPPH inhibition by Ful-incorporated cements (n=5, **=p<0.01, ***= p<0.001, ****= p<0.0001).

Figure 5.8(a) depicts the change in color of DPPH solution after a 24-hour treatment with Ful-incorporated cements. The yellow color observed in the DPPH solution indicates a reduction in DPPH radicals [115] due to the presence of Ful-incorporated cements, while no change was observed in DPPH solutions treated with control and CMC/Gel cements. Figure 5.8(b) presents a quantitative analysis of the reduction in DPPH activity by Ful-incorporated cements, with Ful0.02 and Ful0.04 samples demonstrating 46.58% and 51.41% DPPH inhibition within 24 hours. However, DPPH inhibition was only observed to be 29.28% for the Ful0.1 samples.

Figure 5.9 shows the % viability of MC3T3-E1 cells after treatment with different concentrations of standard Ful particles for 24 hours.

The use of standard Ful particles showed no signs of toxicity in MC3T3-E1 cells when tested in vitro for 24 hours. In fact, at a concentration of 0.250 mg/mL, cellular viability was increased, as shown in Figure 5.9.

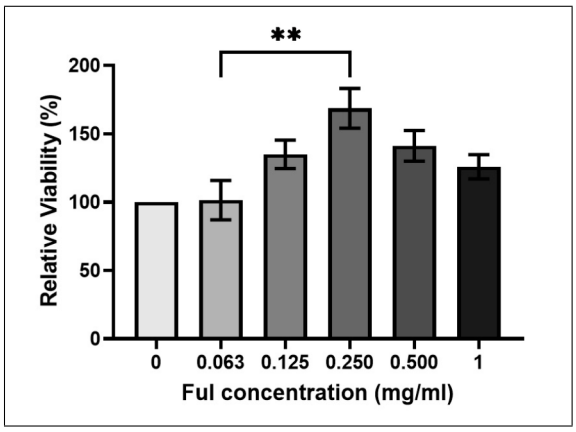

Figure 5.9 Viability of MC3T3-E1 cells after treatment with different concentrations of standard Ful particles for 24 hours.

The in vitro release kinetics of Ful particles from Ful-loaded cements are presented in Figure 5.10.

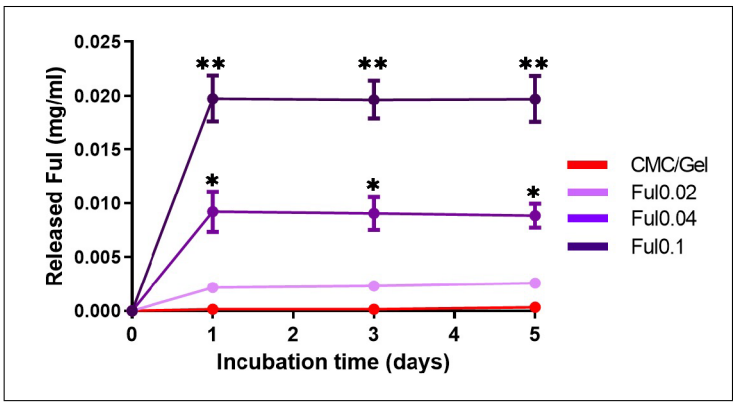

Figure 5.10 In vitro Ful particle release from cements (n=5, * for $p<0.05$ compared to Ful0.02; ** for $p<0.01$ compared to Ful0.02).

Figure 5.10 demonstrates nearly complete release of Ful from the cements within 24 hours. The concentration of cumulative Ful released from the cements was found to be directly proportional to the initial Ful concentration in each sample. It should be noted that Ful concentration released from the cements is lower than the possibly cytotoxic range which is shown in Figure 5.9.

Additionally, excessive quantities of calcium ions can also compromise cellular viability. In vitro release kinetics of Ca ions from cements is presented in Figure 5.11.

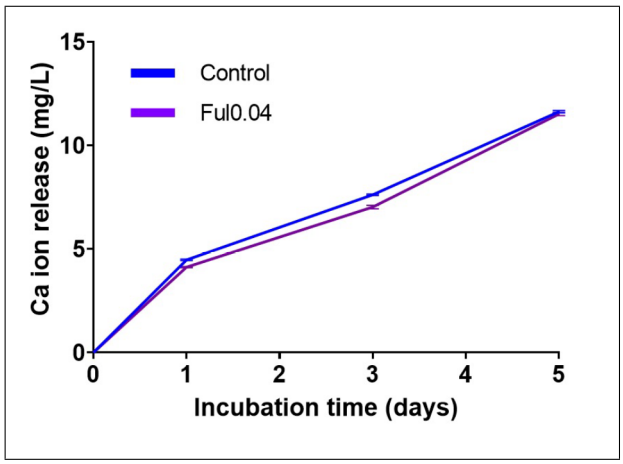

Figure 5.11 In vitro Ca ion release from Ful-incorporated cements (n=4).

In vitro release kinetics of Ca ions from cement formulations demonstrated that less than 12 mg/L of free calcium was released from control or Ful0.04 cements over 5 days.

Furthermore, in vitro cytotoxicity evaluations of Ful-loaded cement extracts were collected from 1, 3, and 5-day incubations and tested in L-929 cells, as shown in Figure 5.12.

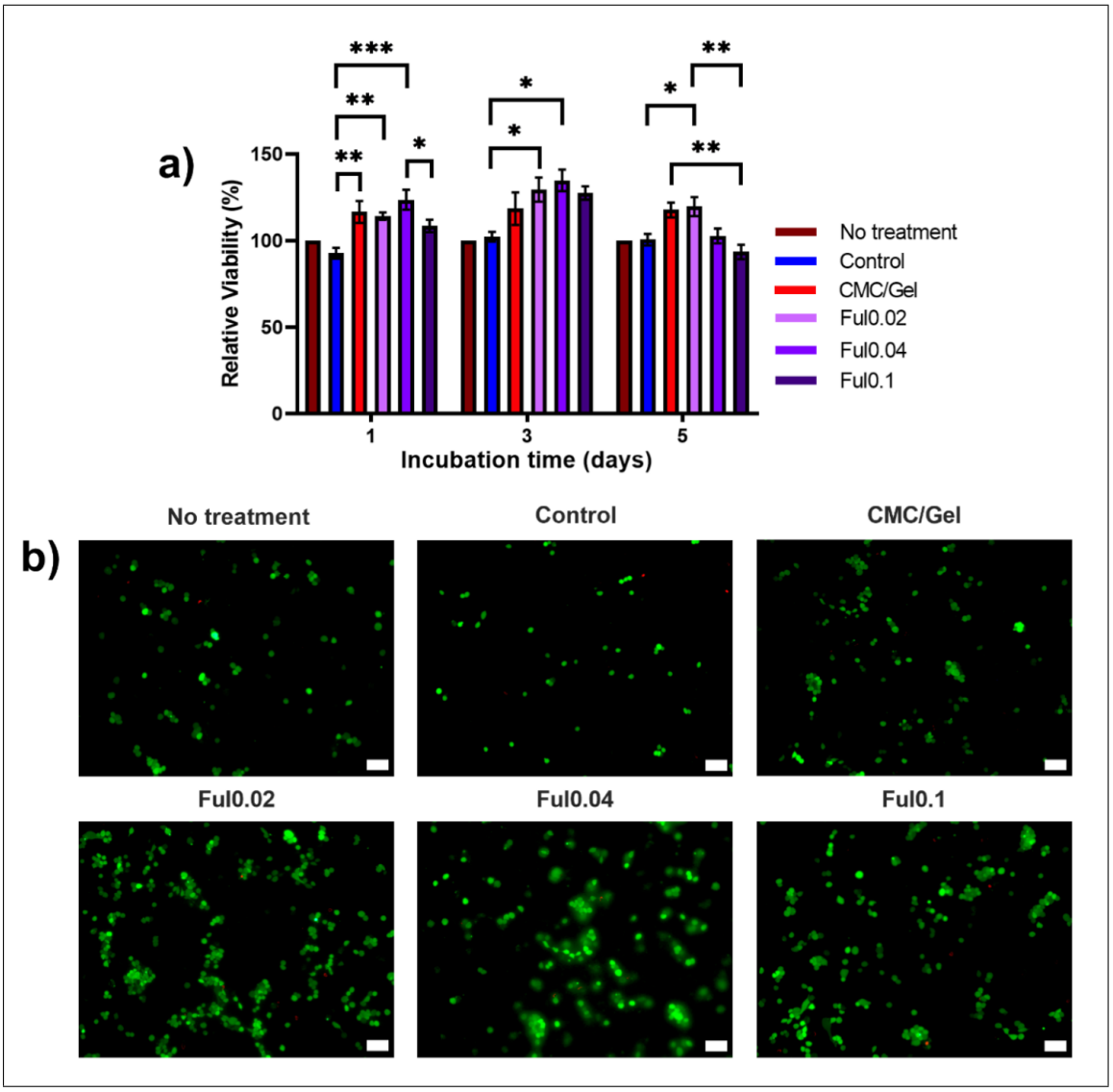

Figure 5.12 (a) Viability of L-929 cells cultured in growth media prepared with control, CMC/Gel, Ful0.02, Ful0.04, and Ful0.1 extracts collected after 1, 3, and 5 days of cement incubation (n=5, *= $p<0.05$, **=$p<0.01$, ***= $p<0.001$). (b) Live-dead staining of L-929 cells cultured in growth media prepared with control, CMC/Gel, Ful0.02, Ful0.04, and Ful0.1 extracts collected after 3-day cement incubation (Scale bars=100 μm, green: live cells, red: dead cells).

The results from day 3 extracts indicate that the cell viability increased with medium-dose Ful particles. The images of extract-treated L-929 with live-dead staining in Figure 5.12(b) support the quantitative viability results in Figure 5.12(a), as Ful0.02 and Ful0.04-treated cells show more coverage than the other treatment groups. Finally, all cement fifth-day extracts were still biocompatible; however, the viability percentage of cells incubated in Ful0.1 fifth-day extracts was significantly lower than cells incubated with CMC/Gel fifth-day extracts.

Figure 5.13 illustrates the impact of Ful-loaded cements on actin fiber intensity of MC3T3-E1 cells after an induction in osteogenic media. cellular osteogenic differentiation.

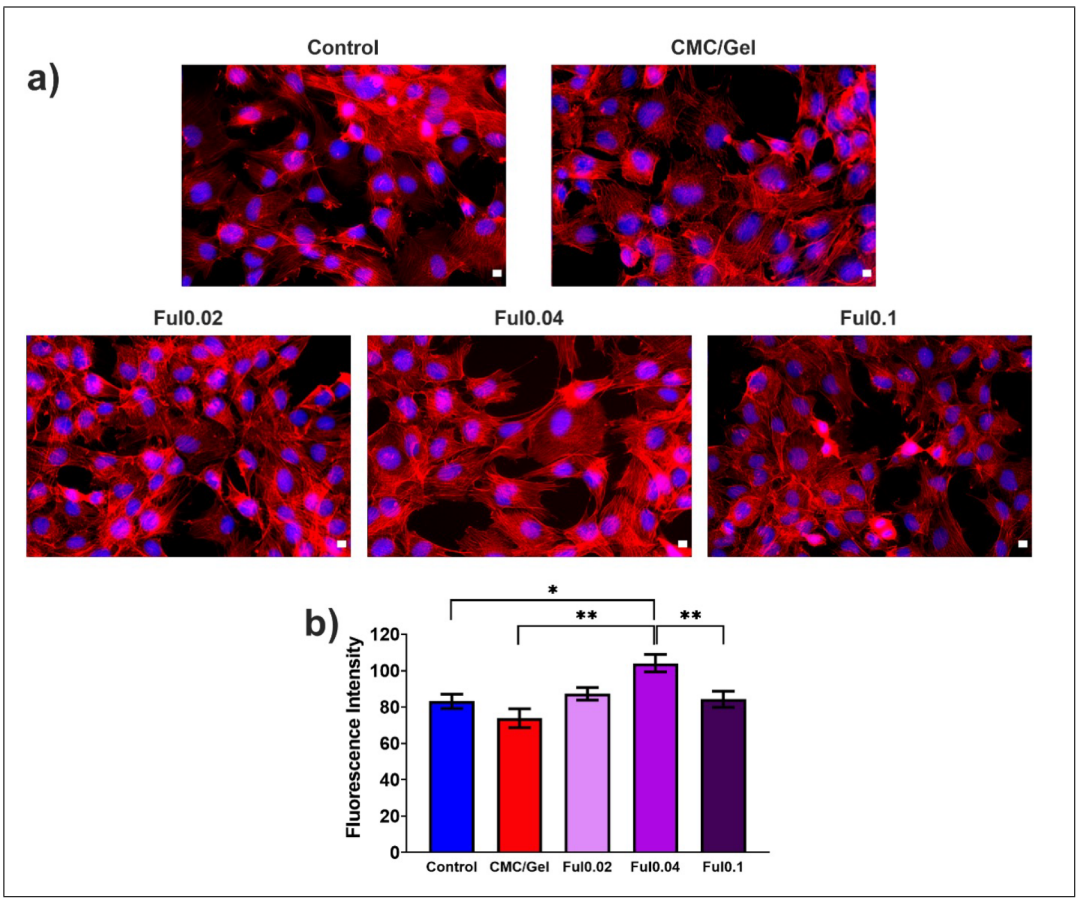

Figure 5.13 (a) Visualization of actin fiber formation following 7-day cement extract treatment via Phalloidin-DAPI staining (scale bars: 10 μm). (b) Average fluorescence intensity of actin fibers after differentiation for 7 days.

Microscopic images in Figure 5.13(a) indicate that Ful0.04-treated cells had denser and more visible actin fibers compared to other cement groups. Furthermore, the quantitative analysis of actin fluorescence intensity (Figure 5.13(b)) confirmed that Ful0.04 significantly increased the actin density of MC3T3-E1 cells, while Ful0.1 decreased it compared to Ful0.04.

The effect of Ful on ALP activity of MC3T3-E1 cells is demonstrated in Figure 5.14.

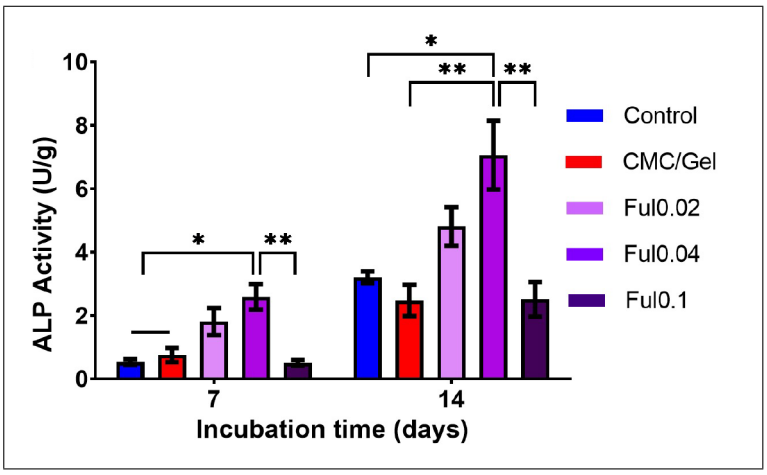

Figure 5.14 ALP activity of cells at days 7 and 14 following treatment with various Ful-incorporated cement extracts (n=3, *= $p<0.05$, **=$p<0.01$).

The ALP activity data supports the findings in 5.13 as Ful0.04 extract media significantly enhanced ALP activity in MC3T3-E1 cells compared to control, CMC/Gel, and Ful0.1 cement extracts. Additionally, ALP production increased over time for all cement extract treatment groups.

The impact of Ful on gene expression is presented in Figure 5.15.

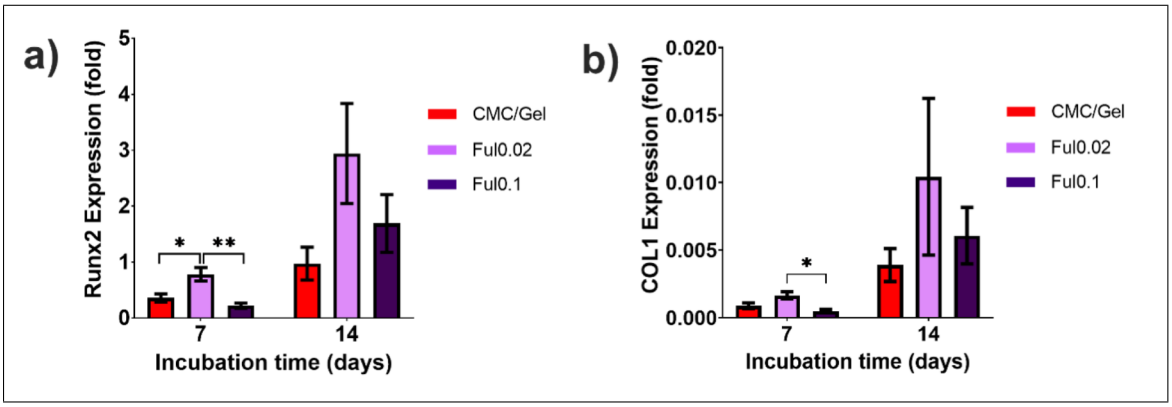

Figure 5.15 (a) Runx2 expression in cells at days 7 and 14 following treatment with various Ful-incorporated cement extracts (n=3, *= $p<0.05$, **=$p<0.01$). (b) COL1 expression in cells at days 7 and 14 following treatment with various Ful-incorporated cement extracts (n=3).

According to the results of gene expression analysis, the gene expression of the osteogenesis marker Runx2 increased between 7 and 14 days for all cement treatment groups, but tripled with low dose Ful treatment (Figure 5.15(a)). However, high dose Ful0.1 cement extracts did not significantly increase Runx2 expression compared to CMC/Gel extracts (Figure 5.15(a)). Finally, low dose Ful cement showed a non-significant increase of COL1 expression, while high dose Ful cement significantly decreased it (Figure 5.15(b)).

5.3 Discussion

This study found that adding the powerful antioxidant Fullerenol enhanced the osteogenic properties of CMC/Gel-blended CPCs. The FTIR analysis showed that the polyhydroxylated Fullerenol molecules strongly interacted with the cement components, specifically through hydrogen bonding with the amine groups from Gel and the carboxyl/hydroxyl groups of CMC, as evidenced by OH-specific peak shifts (Figure 5.1). Previous studies have also shown that Fullerenol can form hydrogen bonds with amino acid amine groups via hydroxyl-amine associations [116, 117, 118]. Furthermore, Dong et al. [117] observed a shift to a lower frequency in the OH band from an FTIR spectra of phenylalanine/Fullerenol due to hydrogen bonding between the amine group of phenylalanine and Fullerenol hydroxyl units. Additionally, Lombo-Vidal et al. [119] reported hydrogen bonding of Fullerenol with carboxyl and hydroxyl groups of polysaccharides. In summary, the demonstrated molecular associations between Fullerenol particles and CMC/Gel cement components are well-supported by previous studies.

The baseline CPCs had an initial/final setting time of 11.4/14 minutes (Figure 5.2), which was increased significantly due to the addition of CMC/Gel, leading to immobilization of TTCP and DCPD particles from the viscosity increase [3, 120]. Interestingly, high concentrations of Ful acted as a facilitator to decrease the setting time of CMC/Gel CPCs. Although the addition of 0.02 and 0.04 wt/v% Ful did not change the initial and final setting times of CMC/Gel cements, the inclusion of 0.1 wt/v% Ful significantly reduced the initial and final setting times, bringing them closer to the clinically recommended time frames [3, 91] (Figure 5.2). The increased cement reactivity is possibly due to an increase in the common ion effect through the hydrogen bonding of Ful particles to $HPO_4{}^{-2}$ [121], as suggested in previous studies on the interaction of hydroxyl groups with phosphates [118]. Thus, these results indicate that $HPO_4{}^{-2}$ sites on Ful0.1 facilitated the binding of Ca^{+2} ions, promoting apatite nucleation in these Ful-doped cement formulations.

Although Ful inclusion in CPC cements led to a decrease in their setting time, it

did not have a significant impact on the conversion rate of TTCP and DCPD particles into CDHA domains, as shown in Figure 5.3 and Figure 5.5. Moreover, the other physical characteristic of the CMC/Gel cements which is compressive strength did not alter via Ful incorporation. All formulations surpassed the benchmark values of 2 MPa for strength and 150 MPa for modulus (Figure 5.7). These results suggest that Ful-doped cements are mechanically appropriate for treating non-load bearing bone reconstructions. (The detailed discussion for apatite formation rate and compressive strength is given in the Section 4.3) The incorporation of Ful into cements demonstrated a significant scavenging of ROS, as determined from the inhibition of the radical molecule DPPH (Figure 5.8). Control and CMC/Gel cement formulations did not exhibit ROS scavenging, whereas low and medium-dose Ful cements showed notable antioxidant activity. However, the highest Ful0.1 dose cements showed reduced ROS scavenging, which could be due to Ful aggregation, as previously described by Roy et al. [122] for these particles at high concentrations [123, 122]. As hydroxyl groups play a significant role in both aggregation and radical scavenging [73], it is suggested that Ful particle aggregation reduces the presentation of active sites on the surface of Ful particles, thereby reducing their interaction with radicals [123, 122].

The cytotoxicity of Ful particle solutions and extracts from Ful-loaded cements was assessed (Figure 5.9 and 5.12), and it was found that no concentration of Ful up to 1 mg/mL was toxic, consistent with previous studies [75, 124, 77, 78, 79, 80, 125] Moreover, at a concentration of 0.25 mg/mL, Ful was found to increase the viability of MC3T3-E1 cells over 24 hours (Figure 5.9). The literature emphasizes that Ful is highly biocompatible [75, 124, 77, 78, 79, 80, 125], and previous evaluations with Ful concentrations up to 10 mg/mL demonstrated non-cytotoxicity using human skin fibroblasts [79, 80], murine macrophage cells [125], and human epidermal keratinocytes [78].

Ful particles were found to be minimally cytotoxic in baseline concentrations, and Ful particles released from cements also demonstrated low cytotoxicity, as demonstrated in Figure 5.12. Burst release of Ful particles from CMC/Gel cements was observed in in vitro release studies over a 24-hour period, which is a common phe-

nomenon [61, 69] due to Ful particles tending to accumulate on the surface of these cements. Quick release kinetics of antioxidant molecules from CPCs were also reported for trolox [69] and selenium [61]. The released Ful particles showed negligible toxicity over time, while day 3 extracts of Ful0.02 and Ful0.04 increased the number of viable L-929 cells, as demonstrated in Figure 5.12(a,b). It was observed that the increase in cell viability could be due to the protective effects of Ful against toxicity from excess CPC-released calcium ions, which can be harmful to cells [126]. Although quantified in vitro calcium ion release from control and Ful0.04 cements indicated that calcium levels were substantially below typical cytotoxic levels [127], it did increase between the first and fifth days of incubation. The higher viability levels for cells treated with Ful0.02 and Ful0.04 extracts were likely due to Ful's antioxidant capacity, which has been demonstrated in other studies. The cell protective effect of Ful is correlated with its ROS scavenging ability, and Ful has been shown to increase the expression of MAPK-related proteins p38 and ERK to suppress ROS-induced toxicity. Ful0.1 cements demonstrated lower levels of ROS scavenging than Ful0.02 and Ful0.04 cements, which closely correlated with lower cell viability after treatment with day 5 Ful0.1 cement extracts. It can be concluded that the high antioxidant capacity of Ful0.02 and Ful0.04 formulations facilitated the increased survival of L-929 cells.

The osteogenic potential of Ful particles delivered from CMC/Gel cements was evaluated through in vitro IF staining, ALP production measurement, and gene expression studies using MC3T3-E1 pre-osteoblasts. Results from IF staining indicated that the fluorescence intensity of actin increased in cells treated with Ful-incorporated cement extracts (Figure 5.13), indicating that Ful0.04 extracts had the strongest osteogenic impact on MC3T3-E1 cells compared to other cement extract treatments. However, in cells incubated with Ful0.1 extracts, F-actin organization was not significantly increased compared to CMC/Gel formulations (Figure 5.13), indicating that Ful particles were possibly aggregating at this higher concentration. Similarly, quantification of cellular ALP production following cement extract treatment largely mirrored the results of IF staining, as shown in Figure 5.14. Extracts from low-dose Ful cements increased cellular ALP levels at both 7 and 14 days and Runx2 gene expression levels at day 7, while the highest dose Ful0.1 cements did not show significant increases in

these osteogenesis markers (Figures 5.14 and 5.15).

Studies have demonstrated that during osteogenic differentiation, antioxidant enzymes suppress ROS levels [128] and numerous in vitro and in vivo studies suggest that antioxidants can accelerate osteogenic differentiation by reducing ROS concentrations [68, 74, 129, 130]. Ful's effect on osteogenic differentiation has also been studied in previous research, with some studies showing that Ful particles can enhance the expression of osteogenic markers such as Runx2, ALP, and OCN, as well as cellular mineralization. These studies suggest that the antioxidant capacity of ROS-scavenging particles correlates with their osteogenic ability. The data from this study (Figure 5.8 and Figure 5.13-5.15) supports this correlation and further analysis is needed to determine the specific mechanisms linking Ful's antioxidant activity to bone formation. ROS interacts with several key osteogenic pathways, including Wnt, FOXO, Hedgehog, and MAPK/ERK [60, 74, 76], and in vivo studies with Ful-loaded CPCs are required to demonstrate its efficacy in bone healing. Nevertheless, this study provides compelling evidence of the benefits Ful can offer to CMC/Gel cements for use in bone reconstruction procedures.

5.4 Conclusion

As an independent process from the synthesis of ND-containing cements, the antioxidant compound Ful was successfully incorporated into the calcium phosphate cementing agent without affecting the apatite formation time, morphology, or compressive strength of the cement. The presence of low concentrations of Ful had no impact on the hardening rates of the cement, while high concentrations resulted in a significant decrease in setting times. Importantly, the Ful-loaded cements exhibited strong antioxidant activity, as demonstrated by DPPH radical scavenging assays. This increased antioxidant activity corresponded to enhanced osteogenic differentiation of MC3T3-E1 pre-osteoblast cells, as indicated by actin network staining, ALP production measurements and expression of Runx2 and COL1. However, it was observed that at high concentrations, Ful's antioxidant activity decreased (possibly due to its aggregation) and resulted in lower levels of cellular osteogenesis. Overall, these findings demonstrate that Ful promotes earlier and more powerful cellular osteogenic differentiation compared to unmodified calcium phosphate cements, without compromising the physical characteristics of the cement.

6. CONCLUSION

- An apatite CPC was synthesized with an apatite formation time less than three hours which is one of the fastest apatite formation time in the literature.

- CMC and Gel were added to cements to improve handling properties and compressive strength, respectfully.

- For further improvement of cements, carbon nanomaterials were added to cements. Unfunctionalized ND was added to CMC/Gel cements to increase their compressive strength and Ful was added to cements to enhance their osteogenic ability.

- The incorporation of ND at high concentrations was found to reduce the setting time of CMC/Gel cements while it did not alter the rate of apatite formation.

- The inclusion of unfunctionalized ND particles did not contribute to the compressive strength and modulus of the cements. This observation can be attributed to the non-uniformity of the liquid phases caused by the aggregation of ND. Therefore, the overall findings suggest that the use of unfunctionalized ND particles effectively decreases the setting time of the cements without compromising the overall duration of apatite formation. However, it is important to prevent the aggregation of ND particles to observe the impact of ND on the compressive strength of the cement.

- High concentrations of Ful significantly reduced the setting time of CMC/Gel cements; however, this incorporation did not affect the apatite formation time.

- Ful addition to CMC/Gel cements did not alter the compressive strength and modulus of the cements.

- Ful-loaded cements exhibited robust antioxidant activity, as evidenced by DPPH radical scavenging assays.

- The increased antioxidant activity was correlated with enhanced osteogenic differentiation of MC3T3-E1 pre-osteoblast cells, as indicated by actin network staining, ALP production measurements, and PCR gene expression analyses.

- Ful's antioxidant activity decreased at high concentrations, possibly due to its aggregation, resulting in lower levels of cellular osteogenesis.

Future work is required to develop a method to functionalize ND particles. Functionalization of ND will prevent the agglomeration of ND particles and facilitate the increase ND concentration in liquid phase [57, 47]. Therefore, functionalization of ND particles will be useful to observe the contribution of ND particles to compressive strength of CPCs.

In addition to the future work with ND particles, future investigations will ascertain the precise mechanisms linking Ful's antioxidant activity to bone formation, considering that ROS interact with various crucial osteogenic pathways such as Wnt, FOXO, Hedgehog, and MAPK/ERK [60, 74, 76]. Additionally, *in vivo* studies utilizing Ful-loaded CPCs in conventional rodent models like calvarial defects [41, 42] or femoral segmental defects [131] are necessary to validate the effectiveness of Ful in promoting bone healing.

APPENDIX A. APATITE FORMATION TIME OF TTCP AND DCPD PARTICLES DEPENDING ON THE PARTICLE SIZE AND LIQUID PHASE

Table A.1
Apatite formation time of TTCP and DCPD particles depending on the particle size and liquid phase.

	Particle size of TTCP and DCPD (μm) / Liquid phase	Conversion time (hours)
This study	TTCP: 5.1 DCPD: 0.162 / Sodium phosphate	3
Neira et al. [93]	TTCP: 1.5 DCPD: 1.1 / Distilled water	6
Burguera et al. [94, 95]	TTCP: 17 DCPD: 1.7 / Sodium phosphate	>24

APPENDIX B. THE EFFECT OF ND-CONTAINING CMC/GEL CEMENTS ON VIABILITY OF HUMAN BONE MARROW-DERIVED MESENCHYMAL STEM CELLS

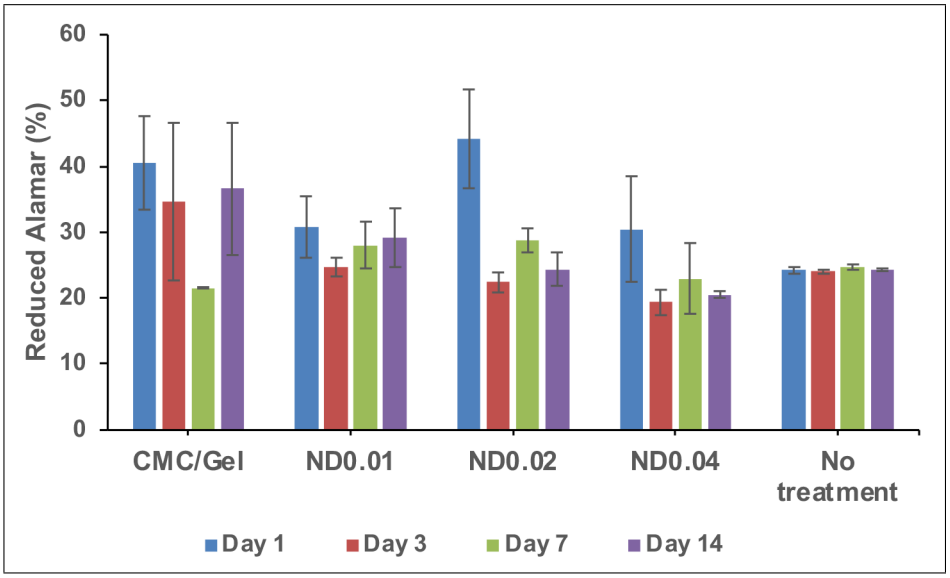

REFERENCES

1. Xia, Y., H. Chen, Y. Zhao, F. Zhang, X. Li, L. Wang, M. D. Weir, J. Ma, M. A. Reynolds, N. Gu, and H. H. Xu, "Novel magnetic calcium phosphate-stem cell construct with magnetic field enhances osteogenic differentiation and bone tissue engineering," *Materials Science and Engineering C*, Vol. 98, pp. 30–41, 5 2019.

2. Golz, T., C. R. Graham, L. C. Busch, J. Wulf, and R. J. Winder, "Temperature elevation during simulated polymethylmethacrylate (pmma) cranioplasty in a cadaver model," *Journal of Clinical Neuroscience*, Vol. 17, pp. 617–622, 5 2010.

3. Perez, R. A., H. W. Kim, and M. P. Ginebra, "Polymeric additives to enhance the functional properties of calcium phosphate cements," *Journal of Tissue Engineering*, Vol. 3, pp. 1–20, 2012.

4. Cherng, A., S. Takagi, and L. C. Chow, "Effects of hydroxypropyl methylcellulose and other gelling agents on the handling properties of calcium phosphate cement," *Journal of Biomedical Materials Research*, Vol. 35, pp. 273–277, 1997.

5. Krebs, J., N. Aebli, B. G. Goss, S. Sugiyama, T. Bardyn, I. Boecken, P. J. Leamy, and S. J. Ferguson, "Cardiovascular changes after pulmonary embolism from injecting calcium phosphate cement," *Journal of Biomedical Materials Research Part B Applied Biomaterials*, Vol. 82, pp. 526–532, 7 2007.

6. Bigi, A., P. Torricelli, M. Fini, B. Bracci, S. Panzavolta, L. Sturba, and R. Giardino, "A biomimetic gelatin-calcium phosphate bone cement," *International Journal of Artificial Organs*, Vol. 27, pp. 664–673, 2004.

7. Li, M., X. Liu, X. Liu, and B. Ge, "Calcium phosphate cement with bmp-2-loaded gelatin microspheres enhances bone healing in osteoporosis: A pilot study," *Clinical Orthopaedics and Related Research*, Vol. 468, pp. 1978–1985, 2010.

8. Bose, S., and S. Tarafder, "Calcium phosphate ceramic systems in growth factor and drug delivery for bone tissue engineering: A review," *Acta Biomaterilia*, Vol. 8, pp. 1401–1421, 2012.

9. Kobayashi, H., T. Fujishiro, S. M. Belkoff, N. Kobayashi, A. S. Turner, H. B. Seim, J. Zitelli, M. Hawkins, and T. W. Bauer, "Long-term evaluation of a calcium phosphate bone cement with carboxymethyl cellulose in a vertebral defect model," *Journal of Biomedical Materials Research - Part A*, Vol. 88, pp. 880–888, 2009.

10. Güben, E., and D. Ege, "Physico-chemical effects of gelatin addition in carboxymethylcellulose and calcium phosphate cement-based nanocomposites," *MRS Advances*, Vol. 357, pp. 1–8, 2019.

11. Devescovi, V., E. Leonardi, G. Ciapetti, and E. Cenni, "Growth factors in bone repair.," *La Chirurgia Degli Organi Di Movimento*, Vol. 92, pp. 161–168, 2008.

12. Campana, V., G. Milano, E. Pagano, M. Barba, C. Cicione, G. Salonna, W. Lattanzi, and G. Logroscino, "Bone substitutes in orthopaedic surgery: from basic science to clinical practice," *Journal of Materials Science: Materials in Medicine*, Vol. 25, pp. 2445–2461, 9 2014.

13. James, A. W., G. LaChaud, J. Shen, G. Asatrian, V. Nguyen, X. Zhang, K. Ting, and C. Soo, "A review of the clinical side effects of bone morphogenetic protein-2," *Tissue Engineering - Part B: Reviews*, Vol. 22, pp. 284–297, 8 2016.

14. Willems, N. M. B. K., G. E. J. Langenbach, V. Everts, and A. Zentner, "The microstructural and biomechanical development of the condylar bone : a review," *European Journal of Orthodontics*, Vol. 36, pp. 479–485, 2014.

15. Lopes, D., C. Martins-cruz, M. B. Oliveira, and J. F. Mano, "Bone physiology as inspiration for tissue regenerative therapies," *Biomaterials*, Vol. 185, pp. 240–275, 2018.

16. Wubneh, A., E. K. Tsekoura, C. Ayranci, and H. Uludag, "Current state of fabrication technologies and materials for bone tissue engineering," *Acta Biomaterialia*, Vol. 80, pp. 1–30, 2018.

17. Fu, Q., E. Saiz, M. N. Rahaman, and A. P. Tomsia, "Toward strong and tough glass and ceramic scaffolds for bone repair," *Advanced Functional Materials*, Vol. 23, pp. 5461–5476, 11 2013.

18. Gerhardt, L. C., and A. R. Boccaccini, "Bioactive glass and glass-ceramic scaffolds for bone tissue engineering," *Materials*, Vol. 3, pp. 3867–3910, 2010.

19. Bigham-Sadegh, A., and A. Oryan, "Basic concepts regarding fracture healing and the current options and future directions in managing bone fractures," *International Wound Journal*, Vol. 12, pp. 238–247, 6 2015.

20. Li, J. J., C. R. Dunstan, A. Entezari, Q. Li, R. Steck, S. Saifzadeh, A. Sadeghpour, J. R. Field, A. Akey, M. Vielreicher, O. Friedrich, S. I. Roohani-Esfahani, and H. Zreiqat, "A novel bone substitute with high bioactivity, strength, and porosity for repairing large and load-bearing bone defects," *Advanced Healthcare Materials*, Vol. 1801298, pp. 1–14, 2019.

21. Garrido, C. A., S. E. Lobo, F. M. Turíbio, and R. Z. Legeros, "Biphasic calcium phosphate bioceramics for orthopaedic reconstructions: Clinical outcomes," *International Journal of Biomaterials*, Vol. 2011, pp. 1–9, 2011.

22. Garai, S., and A. Sinha, "Biomimetic nanocomposites of carboxymethyl cellulose-hydroxyapatite: Novel three dimensional load bearing bone grafts," *Colloids and Surfaces B: Biointerfaces*, Vol. 115, pp. 182–190, 2014.

23. Brown, W. E., and L. C. Chow, "A new calcium phosphate setting cement," *Journal of Dental Research*, Vol. 62, pp. 672–679, 1983.

24. Brown W. E., C. L. C., "Combinations of sparingly soluble calcium phosphates in slurries and pastes as mineralizers and cements," *US. Patent No. 4612053*, 1986.

25. Galea, L. G., M. Bohner, J. Lemaître, T. Kohler, and R. Müller, "Bone substitute: Transforming beta-tricalcium phosphate porous scaffolds into monetite," *Biomaterials*, Vol. 29, pp. 3400–3407, 8 2008.

26. Xu, H. H. K., M. D. Weir, E. F. Burguera, and A. M. Fraser, "Injectable and macroporous calcium phosphate cement scaffold," *Biomaterials*, Vol. 27, pp. 4279–4287, 2006.

27. Liu, Y., J. Wu, Y. Zhu, and J. Han, "Therapeutic application of mesenchymal stem cells in bone and joint diseases," *Clinical and Experimental Medicine*, Vol. 14, pp. 13–24, 2014.

28. Arıcı, Ş., E. G. Kaçmaz, A. R. Kamali, and D. Ege, "Influence of graphene oxide and carbon nanotubes on physicochemical properties of bone cements," *Materials Chemistry and Physics*, Vol. 293, pp. 126961–126971, 2023.

29. Bohner, M., "Reactivity of calcium phosphate cements," *Journal of Materials Chemistry*, Vol. 17, pp. 3980–3986, 2007.

30. Tenhuisen, K. S., and P. W. Brown, "The kinetics of calcium deficient and stoichiometric hydroxyapatite formation from $CaHPO_4$ and $Ca_4(PO_4)_2O$," *Journal of Materials Science: Materials in Medicine*, Vol. 7, pp. 309–316, 1996.

31. Brown, P. W., and M. Fulmer, "Kinetics of hydroxyapatite formation at low temperature," *Journal of the American Ceramic Society*, Vol. 74, pp. 934–940, 1991.

32. Fukase, Y., E. D. Eanes, S. Takagp, L. C. Chow, and W. E. Brown, "Setting reactions and compressive strengths of calcium phosphate cements," *Journal of Dental Research*, Vol. 69, pp. 1852–1856, 1990.

33. Pilia, M., T. Guda, and M. Appleford, "Development of composite scaffolds for load-bearing segmental bone defects," *BioMed Research International*, Vol. 2013, pp. 1–15, 2013.

34. Bigi, A., B. Bracci, and S. Panzavolta, "Effect of added gelatin on the properties of calcium phosphate cement," *Biomaterials*, Vol. 25, pp. 2893–2899, 2004.

35. Y. Fujishiro, K. Takahashi, T. S., "Preparation and compressive strength of α-tricalcium phosphate/gelatin gel composite cement," *Journal of Biomedical Materials Research*, Vol. 54, pp. 525–530, 2000.

36. Lee, S. K., S. K. Lee, S. I. Lee, J. H. Park, J. H. Jang, H. W. Kim, and E. C. Kim, "Effect of calcium phosphate cements on growth and odontoblastic differentiation in human dental pulp cells," *Journal of Endodontics*, Vol. 36, pp. 1537–1542, 2010.

37. Wang, X., J. Ma, Y. Wang, and B. He, "Structural characterization of phosphorylated chitosan and their applications as e!ective additives of calcium phosphate cements," *Biomaterials*, Vol. 22, pp. 2247–2255, 2001.

38. He, H., H. Ren, Z. Ding, M. Ji, H. Chen, and Y. Yan, "Developing a novel magnesium calcium phosphate/sodium alginate composite cement with high strength and proper self-setting time for bone repair," *Journal of Biomaterials Applications*, Vol. 36, pp. 346–357, 8 2021.

39. Blom, E. J., J. Klein-Nulend, C. P. A. T. Klein, K. Kurashina, M. A. J. V. Waas, and E. H. Burger, "Transforming growth factor-1 incorporated during setting in calcium phosphate cement stimulates bone cell differentiation in vitro," *J Biomed Mater Res.*, Vol. 50, pp. 67–74, 2000.

40. Gillman, C. E., and A. C. Jayasuriya, "Fda-approved bone grafts and bone graft substitute devices in bone regeneration," *Materials Science and Engineering C*, Vol. 130, 11 2021.

41. Wu, X., Z. Tang, K. Wu, Y. Bai, X. Lin, H. Yang, Q. Yang, Z. Wang, X. Ni, H. Liu, and L. Yang, "Strontium-calcium phosphate hybrid cement with enhanced osteogenic and angiogenic properties for vascularised bone regeneration," *Journal of Materials Chemistry B*, Vol. 9, pp. 5982–5997, 8 2021.

42. Ding, S., J. Zhang, Y. Tian, B. Huang, Y. Yuan, and C. Liu, "Magnesium modification up-regulates the bioactivity of bone morphogenetic protein-2 upon calcium phosphate cement via enhanced bmp receptor recognition and smad signaling pathway," *Colloids and Surfaces B: Biointerfaces*, Vol. 145, pp. 140–151, 9 2016.

43. Seonwoo, H., H. W. Choung, S. Park, K. S. Choi, K. J. Jang, J. Kim, K. T. Lim, Y. Kim, P. Garg, S. Pandey, J. Lee, J. C. Park, Y. H. Choung, P. H. Choung, S. Y. Kim, and J. H. Chung, "Reduced graphene oxide-incorporated calcium phosphate cements with pulsed electromagnetic fields for bone regeneration," *RSC Advances*, Vol. 12, pp. 5557–5570, 1 2022.

44. Chauhan, S., N. Jain, and U. Nagaich, "Nanodiamonds with powerful ability for drug delivery and biomedical applications: Recent updates on in vivo study and patents," *Journal of Pharmaceutical Analysis*, Vol. 10, pp. 1–12, 2 2020.

45. Xing, Z., T. O. Pedersen, X. Wu, Y. Xue, Y. Sun, A. Finne-Wistrand, F. R. Kloss, T. Waag, A. Krueger, D. Steinmüller-Nethl, and K. Mustafa, "Biological effects of functionalizing copolymer scaffolds with nanodiamond particles," *Tissue Engineering Part A*, Vol. 19, pp. 1783–1791, 2013.

46. Pacelli, S., R. Maloney, A. R. Chakravarti, J. Whitlow, S. Basu, S. Modaresi, S. Gehrke, and A. Paul, "Controlling adult stem cell behavior using nanodiamond-reinforced hydrogel: Implication in bone regeneration therapy," *Scientific Reports*, Vol. 7, pp. 1–15, 2017.

47. Zhang, Q., V. N. Mochalin, I. Neitzel, I. Y. Knoke, J. Han, C. A. Klug, J. G. Zhou, P. I. Lelkes, and Y. Gogotsi, "Fluorescent plla-nanodiamond composites for bone tissue engineering," *Biomaterials*, Vol. 32, pp. 87–94, 2011.

48. Shuai, C., W. Huang, P. Feng, C. Gao, D. Gao, Y. Deng, Q. Wang, P. Wu, and X. Guo, "Nanodiamond reinforced polyvinylidene fluoride/bioglass scaffolds for bone tissue engineering," *Journal of Porous Materials*, Vol. 24, pp. 249–255, 2017.

49. Salaam, A. D., M. Mishra, E. Nyairo, and D. Dean, "Electrospun polyvinyl alcohol/nanodiamond composite scaffolds: Morphological, structural, and biological analysis," *Journal of Biomaterials and Tissue Engineering*, Vol. 4, pp. 1–8, 2014.

50. Suliman, S., Y. Sun, T. O. Pedersen, Y. Xue, J. Nickel, T. Waag, A. Finne-Wistrand, D. Steinmüller-Nethl, A. Krueger, D. E. Costea, and K. Mustafa, "In vivo host response and degradation of copolymer scaffolds functionalized with nanodiamonds and bone morphogenetic protein 2," *Advanced Healthcare Materials*, Vol. 5, pp. 730–742, 2016.

51. Sun, Y., A. Finne-Wistrand, T. Waag, Z. Xing, M. Yassin, A. Yamamoto, K. Mustafa, D. Steinmüller-Nethl, A. Krueger, and A. C. Albertsson, "Reinforced degradable biocomposite by homogenously distributed functionalized nanodiamond particles," *Macromolecular Materials and Engineering*, Vol. 300, pp. 436–447, 2015.

52. Suliman, S., Z. Xing, X. Wu, Y. Xue, T. O. Pedersen, Y. Sun, A. P. DÃ¸skeland, J. Nickel, T. Waag, H. Lygre, A. Finne-Wistrand, D. Steinmüller-Nethl, A. Krueger, and K. Mustafa, "Release and bioactivity of bone morphogenetic protein-2 are affected by scaffold binding techniques in vitro and in vivo," *Journal of Controlled Release*, Vol. 197, pp. 148–157, 2015.

53. Yassin, M. A., K. Mustafa, Z. Xing, Y. Sun, K. E. Fasmer, T. Waag, A. Krueger, D. Steinmüller-Nethl, A. Finne-Wistrand, and K. N. Leknes, "A copolymer scaffold functionalized with nanodiamond particles enhances osteogenic metabolic activity and bone regeneration," *Macromolecular Bioscience*, Vol. 17, pp. 1–11, 2017.

54. Salaam, A. D., and D. Dean, "Electrospun polycaprolactone-nanodiamond composite scaffolds for bone tissue engineering," *Proceedings of ASME 2010 First Global Congress on NanoEngineering for Medicine and Biology Proceedings of NEMB2010*, pp. 1–4, 2010.

55. Parizek, M., T. E. Douglas, K. Novotna, A. Kromka, M. A. Brady, A. Renzing, E. Voss, M. Jarosova, L. Palatinus, P. Tesarek, P. Ryparova, V. Lisa, A. M. dos Santos, and L. Bacakova, "Nanofibrous poly(lactide-co-glycolide) membranes loaded with diamond nanoparticles as promising substrates for bone tissue engineering," *International Journal of Nanomedicine*, Vol. 7, pp. 1931–1951, 2012.

56. Brady, M. A., A. Renzing, T. E. L. Douglas, Q. Liu, S. Wille, M. Parizek, L. Bacakova, A. Kromka, M. Jarosova, G. Godier, and P. H. Warnke, "Development of composite poly(lactide-co-glycolide)-nanodiamond scaffolds for bone cell growth," *Journal of Nanoscience and Nanotechnology*, Vol. 15, pp. 1060–1069, 2015.

57. Alishiri, M., A. Shojaei, and M. J. Abdekhodaie, "Biodegradable polyurethane acrylate/hema-grafted nanodiamond composites with bone regenerative potential applications: structure, mechanical properties and biocompatibility," *RSC Adv.*, Vol. 6, pp. 8743–8755, 2016.

58. Serafim, A., S. Cecoltan, A. Lungu, E. Vasile, H. Iovu, and I. C. Stancu, "Electrospun fish gelatin fibrous scaffolds with improved bio-interactions due to carboxylated nanodiamond loading," *RSC Adv.*, Vol. 5, pp. 95467–95477, 2015.

59. Zhang, Q., V. N. Mochalin, I. Neitzel, K. Hazeli, J. Niu, A. Kontsos, J. G. Zhou, P. I. Lelkes, and Y. Gogotsi, "Mechanical properties and biomineralization of multifunctional nanodiamond-plla composites for bone tissue engineering," *Biomaterials*, Vol. 33, pp. 5067–5075, 2012.

60. Atashi, F., A. Modarressi, and M. S. Pepper, "The role of reactive oxygen species in mesenchymal stem cell adipogenic and osteogenic differentiation: A review," *Stem Cells and Development*, Vol. 24, pp. 1150–1163, 2015.

61. Pujari-Palmer, S., X. Lu, V. P. Singh, L. Engman, M. Pujari-Palmer, and M. K. Ott, "Incorporation and delivery of an organoselenium antioxidant from a brushite cement," *Materials Letters*, Vol. 197, pp. 115–119, 2017.

62. Hatanaka, E., A. Dermargos, H. A. Armelin, R. Curi, and A. Campa, "Serum amyloid a induces reactive oxygen species (ros) production and proliferation of fibroblast," *Clinical and Experimental Immunology*, Vol. 163, pp. 362–367, 2011.

63. Cao, S., Y. Zhao, Y. Hu, L. Zou, and J. Chen, "New perspectives: In-situ tissue engineering for bone repair scaffold," *Composites Part B: Engineering*, Vol. 202, p. 108445, 2020.

64. Pinna, A., M. T. Baghbaderani, V. V. HernÃ¡ndez, P. Naruphontjirakul, S. Li, T. McFarlane, D. Hachim, M. M. Stevens, A. E. Porter, and J. R. Jones, "Nanoceria provides antioxidant and osteogenic properties to mesoporous silica nanoparticles for osteoporosis treatment," *Acta Biomaterialia*, Vol. 122, pp. 365–376, 3 2021.

65. Liu, M., X. Wu, Y. Cui, P. Liu, B. Xiao, X. Zhang, J. Zhang, Z. Sun, M. Song, B. Shao, and Y. Li, "Mitophagy and apoptosis mediated by ros participate in alcl3-induced mc3t3-e1 cell dysfunction," *Food and Chemical Toxicology*, Vol. 155, p. 112388, 9 2021.

66. Tao, H., G. Ge, X. Liang, W. Zhang, H. Sun, M. Li, and D. Geng, "Ros signaling cascades: Dual regulations for osteoclast and osteoblast," 10 2020.

67. Kim, S. E., S. Choi, J. Y. Hong, K. S. Shim, T. H. Kim, K. Park, and S. H. Lee, "Accelerated osteogenic differentiation of mc3t3-e1 cells by lactoferrin-conjugated nanodiamonds through enhanced anti-oxidant and anti- inflammatory effects," *Nanomaterials*, Vol. 10, pp. 1–14, 1 2020.

68. Lee, S. C., N. H. Lee, K. D. Patel, T. S. Jang, J. C. Knowles, H. W. Kim, H. H. Lee, and J. H. Lee, "The effect of selenium nanoparticles on the osteogenic differentiation of mc3t3-e1 cells," *Nanomaterials*, Vol. 11, pp. 1–15, 2 2021.

69. Mestres, G., C. F. Santos, L. Engman, C. Persson, and M. K. Ott, "Scavenging effect of trolox released from brushite cements," *Acta Biomaterialia*, Vol. 11, pp. 459–466, 2015.

70. Borut Strukelj Rade Injac, M. P., "Fullerenol nanoparticles: Toxicity and antioxidant activity," *Oxidative Stress and Nanotechnology*, pp. 75–100, 2013.

71. Markovic, Z., and V. Trajkovic, "Biomedical potential of the reactive oxygen species generation and quenching by fullerenes (C_{60})," *Biomaterials*, Vol. 29, pp. 3561–3573, 9 2008.

72. Osuna, S., M. Swart, and M. Solá, "On the mechanism of action of fullerene derivatives in superoxide dismutation," *Chemistry - A European Journal*, Vol. 16, pp. 3207–3214, 2010.

73. Podolsky, N. E., M. A. Marcos, D. Cabaleiro, K. N. Semenov, L. Lugo, A. V. Petrov, N. A. Charykov, V. V. Sharoyko, T. D. Vlasov, and I. V. Murin, "Physico-chemical properties of $C_{60}(OH)_{22-24}$," *Journal of Molecular Liquids*, pp. 342–355, 3.

74. Yang, X., C. J. Li, Y. Wan, P. Smith, G. Shang, and Q. Cui, "Antioxidative fullerol promotes osteogenesis of human adipose-derived stem cells," *International Journal of Nanomedicine*, Vol. 9, pp. 4023–4031, 2014.

75. Hao, T., J. Li, F. Yao, D. Dong, Y. Wang, B. Yang, and C. Wang, "Injectable fullerenol/alginate hydrogel for suppression of oxidative stress damage in brown adipose-derived stem cells and cardiac repair," *ACS Nano*, Vol. 11, pp. 5474–5488, 2017.

76. Liu, H., X. Yang, Y. Zhang, A. Dighe, X. Li, and Q. Cui, "Fullerol antagonizes dexamethasone-induced oxidative stress and adipogenesis while enhancing osteogenesis in a cloned bone marrow mesenchymal stem cell," *Journal of Orthopaedic Research*, Vol. 30, pp. 1051–1057, 11 2012.

77. Lichota, A., I. PiwoÅski, S. Michlewska, and A. Krokosz, "A multiparametric study of internalization of fullerenol $C_{60}(OH)_{36}$ nanoparticles into peripheral blood mononuclear cells: Cytotoxicity in oxidative stress induced by ionizing radiation," *International Journal of Molecular Sciences*, Vol. 21, pp. 1–18, 4 2020.

78. Saathoff, J. G., A. O. Inman, X. R. Xia, J. E. Riviere, and N. A. Monteiro-Riviere, "In vitro toxicity assessment of three hydroxylated fullerenes in human skin cells," *Toxicology in Vitro*, Vol. 25, pp. 2105–2112, 12 2011.

79. Sayes, C. M., J. D. Fortner, W. Guo, D. Lyon, A. M. Boyd, K. D. Ausman, Y. J. Tao, B. Sitharaman, L. J. Wilson, J. B. Hughes, J. L. West, and V. L. Colvin, "The differential cytotoxicity of water-soluble fullerenes," *Nano Letters*, Vol. 4, pp. 1881–1887, 10 2004.

80. Nurzynska, A., P. Piotrowski, K. Klimek, J. Król, A. Kaim, and G. Ginalska, "Novel C_{60} fullerenol-gentamicin conjugateâphysicochemical characterization and evaluation of antibacterial and cytotoxic properties," *Molecules*, Vol. 27, pp. 1–13, 7 2022.

81. Ebrahimi, M., M. Botelho, W. Lu, and N. Monmaturapoj, "Synthesis and characterization of biomimetic bioceramic nanoparticles with optimized physicochemical properties for bone tissue engineering," *Journal of Biomedical Materials Research - Part A*, Vol. 107, pp. 1654–1666, 2019.

82. Tadier, S., N. L. Bolay, C. Rey, and C. Combes, "Co-grinding significance for calcium carbonate-calcium phosphate mixed cement. part i: Effect of particle size and mixing on solid phase reactivity," *Acta Biomaterialia*, Vol. 7, pp. 1817–1826, 2011.

83. ASTM, "Standard test method for time of setting of hydraulic-cement paste by gillmore," *ASTM C266-20*, 2020.

84. Song, H. Y., A. H. E. Rahman, and B. T. Lee, "Fabrication of calcium phosphate-calcium sulfate injectable bone substitute using chitosan and citric acid," *Journal of Materials Science: Materials in Medicine*, Vol. 20, pp. 935–941, 2009.

85. Güben, E., Ş. Arıcı, D. Bayır, E. Bozdağ, and D. Ege, "Preparation of calcium phosphate /carboxymethyl cellulose-based bone cements," *Bioinspired, Biomimetic and Nanomaterials*, Vol. 9, pp. 155–163, 2020.

86. Oğuz, Ö. D., and D. Ege, "Effect of zoledronic acid and graphene oxide on the physical and in vitro properties of injectable bone substitutes," *Materials Science and Engineering: C*, Vol. 120, p. 111758, 2020.

87. Seyedlar, R. M., A. Nodehi, M. Atai, and M. Imani, "Gelation behavior of in situ forming gels based on hpmc and biphasic calcium phosphate nanoparticles," *Carbohydrate Polymers*, Vol. 99, pp. 257–263, 2014.

88. Orshesh, Z., S. Hesaraki, and A. Khanlarkhani, "Blooming gelatin: An individual additive for enhancing nanoapatite precipitation, physical properties, and osteoblastic responses of nanostructured macroporous calcium phosphate bone cements," *International Journal of Nanomedicine*, Vol. 12, pp. 745–758, 2017.

89. Tas, A. C., "Preparation of porous apatite granules from calcium phosphate cement," *Journal of Materials Science: Materials in Medicine*, Vol. 19, pp. 2231–2239, 2008.

90. Espanol, M., J. Portillo, J. M. Manero, and M. P. Ginebra, "Investigation of the hydroxyapatite obtained as hydrolysis product of α-tricalcium phosphate by transmission electron microscopy," *Cryst Eng Comm*, Vol. 12, pp. 3318–3326, 2010.

91. Khairoun, I., M. G. Boltong, F. C. Driessens, and J. A. Planell, "Limited compliance of some apatitic calcium phosphate bone cements with clinical requirements," *Journal of Materials Science: Materials in Medicine*, Vol. 9, pp. 667–671, 1998.

92. Blanchard, J. W., T. L. Groy, J. L. Yarger, and G. P. Holland, "Investigating hydrogen-bonded phosphonic acids with proton ultrafast mas nmr and dft calculations," *Journal of Physical Chemistry C*, Vol. 116, pp. 18824–18830, 9 2012.

93. Neira, I. S., Y. V. Kolen'ko, O. I. Lebedev, G. V. Tendeloo, H. S. Gupta, N. Matsushita, M. Yoshimura, and F. GuitiÃ¡n, "Rational synthesis of a nanocrystalline calcium phosphate cement exhibiting rapid conversion to hydroxyapatite," *Materials Science and Engineering C*, Vol. 29, pp. 2124–2132, 8 2009.

94. Burguera, E., F. Guitián, and L. C. Chow, "A rapid setting ttcp-dcpd cement. study of the setting reaction as a function of time," *Key Engineering Materials*, Vol. 284-286, pp. 15–18, 2005.

95. Burguera, E. F., F. Guitián, and L. C. Chow, "A water setting tetracalcium phosphate-dicalcium phosphate dihydrate cement," *Journal of Biomedical Materials Research - Part A*, Vol. 71, pp. 275–282, 2004.

96. Jang, J. H., S. Shin, H. J. Kim, J. Jeong, H. E. Jin, M. S. Desai, S. W. Lee, and S. Y. Kim, "Improvement of physical properties of calcium phosphate cement by elastin-like polypeptide supplementation," *Scientific Reports*, Vol. 8, pp. 1–11, 2018.

97. Schickert, S. D. L., J. C. Pinto, J. Jansen, S. C. Leeuwenburgh, and J. J. V. D. Beucken, "Tough and injectable fiber reinforced calcium phosphate cement as an alternative to polymethylmethacrylate cement for vertebral augmentation: A biomechanical study," *Biomaterials Science*, Vol. 8, pp. 4239–4250, 2020.

98. Bigi, A., I. Cantelli, S. Panzavolta, and K. Rubini, "α-tricalcium phosphate-gelatin composite," *Journal of Applied Biomaterials Biomechanics*, Vol. 2, pp. 81–87, 2004.

99. Shuai, C., Y. Li, G. Wang, W. Yang, S. Peng, and P. Feng, "Surface modification of nanodiamond: Toward the dispersion of reinforced phase in poly-l-lactic acid scaffolds," *International Journal of Biological Macromolecules*, Vol. 126, pp. 1116–1124, 4 2019.

100. Gong, C., S. Fang, K. Xia, J. Chen, L. Guo, and W. Guo, "Enhancing the mechanical properties and cytocompatibility of magnesium potassium phosphate cement by incorporating oxygen-carboxymethyl chitosan," *Regenerative Biomaterials*, Vol. 8, pp. 1–10, 2020.

101. Kokubo, T., and H. Takadama, "How useful is sbf in predicting in vivo bone bioactivity?," *Biomaterials*, Vol. 27, pp. 2907–2915, 2006.

102. Patil, P., K. A. Russo, J. T. McCune, A. C. Pollins, M. A. Cottam, B. R. Dollinger, C. R. DeJulius, M. K. Gupta, R. DâArcy, J. M. Colazo, F. Yu, M. G. Bezold, J. R. Martin, N. L. Cardwell, J. M. Davidson, C. M. Thompson, A. Barbul, A. H. Hasty, S. A. Guelcher, and C. L. Duvall, "Reactive oxygen species â degradable polythioketal urethane foam dressings to promote porcine skin wound repair," *Science Translational Medicine*, Vol. 14, 4 2022.

103. Martin, J. R., M. K. Gupta, J. M. Page, F. Yu, J. M. Davidson, S. A. Guelcher, and C. L. Duvall, "A porous tissue engineering scaffold selectively degraded by cell-generated reactive oxygen species," *Biomaterials*, Vol. 35, pp. 3766–3776, 2014.

104. Xiao, H., F. Yang, Q. Lin, L. Zhang, S. Sun, W. Zhou, and G.-Q. Liu, "Preparation of fluorescent nanoparticles based on broken-rice starch for live-cell imaging," *International Journal of Biological Macromolecules*, Vol. 217, pp. 88–95, 9 2022.

105. ISO, "Biological evaluation of medical devices part 5: Tests for in vitro cytotoxicity (ISO 10993-5:2009)," 2009.

106. Gong, T., Z. Wang, Y. Zhang, Y. Zhang, M. Hou, X. Liu, Y. Wang, L. Zhao, N. D. Ruse, T. Troczynski, and U. O. Häfeli, "A comprehensive study of osteogenic calcium phosphate silicate cement: Material characterization and in vitro/in vivo testing," *Advanced Healthcare Materials*, Vol. 5, pp. 457–466, 2016.

107. Su, J. J. M., C. H. Lin, H. Chen, S. Y. Lee, and Y. M. Lin, "Biofabrication of cell-laden gelatin methacryloyl hydrogels with incorporation of silanized hydroxyapatite by visible light projection," *Polymers*, Vol. 13, 2021.

108. Chen, Y., N. Kawazoe, and G. Chen, "Preparation of dexamethasone-loaded biphasic calcium phosphate nanoparticles/collagen porous composite scaffolds for bone tissue engineering," *Acta Biomaterialia*, Vol. 67, pp. 341–353, 2018.

109. Sun, C., D. Xu, and D. Xue, "In situ ftir-atr observation of structural dynamics of H_2PO_4 in precrystallisation solution," *Materials Research Innovations*, Vol. 18, pp. 370–375, 2014.

110. Biernacki, K. A., E. Kaczkowska, and P. Bruździak, "Aqueous solutions of nma, Na_2HPO_4, and NaH_2PO_4 as models for interaction studies in phosphateâprotein systems," *Journal of Molecular Liquids*, Vol. 265, pp. 361–371, 2018.

111. Singh, V., and S. Ahmad, "Carboxymethyl cellulose-gelatin-silica nanohybrid: An efficient carrier matrix for alpha amylase," *International Journal of Biological Macromolecules*, Vol. 67, pp. 439–445, 2014.

112. Yang, X., M. Zhen, G. Li, X. Liu, X. Wang, C. Shu, L. Jiang, and C. Wang, "Preparation of pd-decorated fullerenols on carbon nanotubes with excellent electrocatalytic properties in alkaline media," *Journal of Materials Chemistry A*, Vol. 1, pp. 8105–8110, 7 2013.

113. Williamson, M. P., and D. H. Williams, "Hydrophobic interactions affect hydrogen bond strengths in complexes between peptides and vancomycin or ristocetin," *European Journal of Biochemistry*, Vol. 138, pp. 345–348, 1984.

114. Berry, E. E., "The structure and composition of some calcium-deficient apatites-ii," *Journal of Inorganic and Nuclear Chemistry*, Vol. 29, 1967.

115. Rahman, M. M., M. B. Islam, M. Biswas, and A. H. K. Alam, "In vitro antioxidant and free radical scavenging activity of different parts of tabebuia pallida growing in bangladesh," *BMC Research Notes*, Vol. 8, 10 2015.

116. Radic, S., P. Nedumpully-Govindan, R. Chen, E. Salonen, J. M. Brown, P. C. Ke, and F. Ding, "Effect of fullerenol surface chemistry on nanoparticle binding-induced protein misfolding," *Nanoscale*, Vol. 6, pp. 8340–8349, 7 2014.

117. Dong, W. R., G. Chen, Z. X. Chen, and S. P. Deng, "Thermodynamics of the enantiomers of amino acid and monosaccharide binding to fullerenol used as an artificial sweet taste receptor model," *Food Chemistry*, Vol. 141, pp. 3110–3117, 2013.

118. Pinteala, M., A. Dascalu, and C. Ungurenasu, "Binding fullerenol $C_{60}(OH)_{24}$ to dsdna," *International Journal of Nanomedicine*, pp. 193–199, 9 2009.

119. Vidal, O. L., A. Tsukui, R. Garrett, M. H. M. Rocha-LeÃ£o, C. W. P. Carvalho, S. P. Freitas, C. M. de Rezende, and M. S. L. Ferreira, "Production of bioactive films of carboxymethyl cellulose enriched with green coffee oil and its residues," *International Journal of Biological Macromolecules*, Vol. 146, pp. 730–738, 3 2020.

120. Wang, X., J. Ye, Y. Wang, and L. Chen, "Reinforcement of calcium phosphate cement by bio-mineralized carbon nanotube," *Journal of the American Ceramic Society*, Vol. 90, pp. 962–964, 2007.

121. Vente, J. D., P. J. Bruyn, and J. Zaagsma, "Fluorescence spectroscopic analysis of the hydrogen bonding properties of catecholamines, resorcinolamines, and related compounds with phosphate and other anionic species in aqueous solution," *Journal of Pharmacy and Pharmacology*, Vol. 33, pp. 290–296, 1981.

122. Roy, P., S. Bag, D. Chakraborty, and S. Dasgupta, "Exploring the inhibitory and antioxidant effects of fullerene and fullerenol on ribonuclease a," *ACS Omega*, Vol. 3, pp. 12270–12283, 9 2018.

123. Jeng, U. S., W. J. Liu, T. L. Lin, L. Y. Wang, and L. Y. Chiang, "Fractal structure of polyhydroxylated fullerenes in water solutions," *Fullerene Science and Technology*, Vol. 7, pp. 599–608, 1999.

124. Geng, H., Y. N. Chang, X. Bai, S. Liu, Q. Yuan, W. Gu, J. Li, K. Chen, G. Xing, and G. Xing, "Fullerenol nanoparticles suppress rankl-induced osteoclastogenesis by inhibiting differentiation and maturation," *Nanoscale*, Vol. 9, pp. 12516–12523, 2017.

125. Chen, Y.-W., K. C. Hwang, C.-C. Yen, and Y.-L. Lai, "Fullerene derivatives protect against oxidative stress in raw 264.7 cells and ischemia-reperfused lungs," *Am J Physiol Regul Integr Comp Physiol*, Vol. 287, pp. 21–26, 2004.

126. Link, D. P., J. V. D. Dolder, J. G. Wolke, and J. A. Jansen, "The cytocompatibility and early osteogenic characteristics of an injectable calcium phosphate cement," *Tissue Engineering*, Vol. 13, pp. 493–500, 3 2007.

127. Epple, M., "Review of potential health risks associated with nanoscopic calcium phosphate," *Acta Biomaterialia*, Vol. 77, pp. 1–14, 9 2018.

128. Chen, C.-T., Y.-R. V. Shih, T. K. Kuo, O. K. Lee, and Y.-H. Wei, "Coordinated changes of mitochondrial biogenesis and antioxidant enzymes during osteogenic differentiation of human mesenchymal stem cells," *Stem Cells*, Vol. 26, pp. 960–968, 2008.

129. Battin, E. E., and J. L. Brumaghim, "Antioxidant activity of sulfur and selenium: A review of reactive oxygen species scavenging, glutathione peroxidase, and metal-binding antioxidant mechanisms," *Cell Biochemistry and Biophysics*, Vol. 55, pp. 1–23, 7 2009.

130. Yamada, M., N. Tsukimura, T. Ikeda, Y. Sugita, W. Att, N. Kojima, K. Kubo, T. Ueno, K. Sakurai, and T. Ogawa, "N-acetyl cysteine as an osteogenesis-enhancing molecule for bone regeneration," *Biomaterials*, Vol. 34, pp. 6147–6156, 2013.

131. Baier, M., P. Staudt, R. Klein, U. Sommer, R. Wenz, I. Grafe, P. J. Meeder, P. P. Nawroth, and C. Kasperk, "Strontium enhances osseointegration of calcium phosphate cement: A histomorphometric pilot study in ovariectomized rats," *Journal of Orthopaedic Surgery and Research*, Vol. 8, 6 2013.